Cell Reports

Article

Chronic stress physically spares but functionally impairs innate-like invariant T cells

Graphical abstract

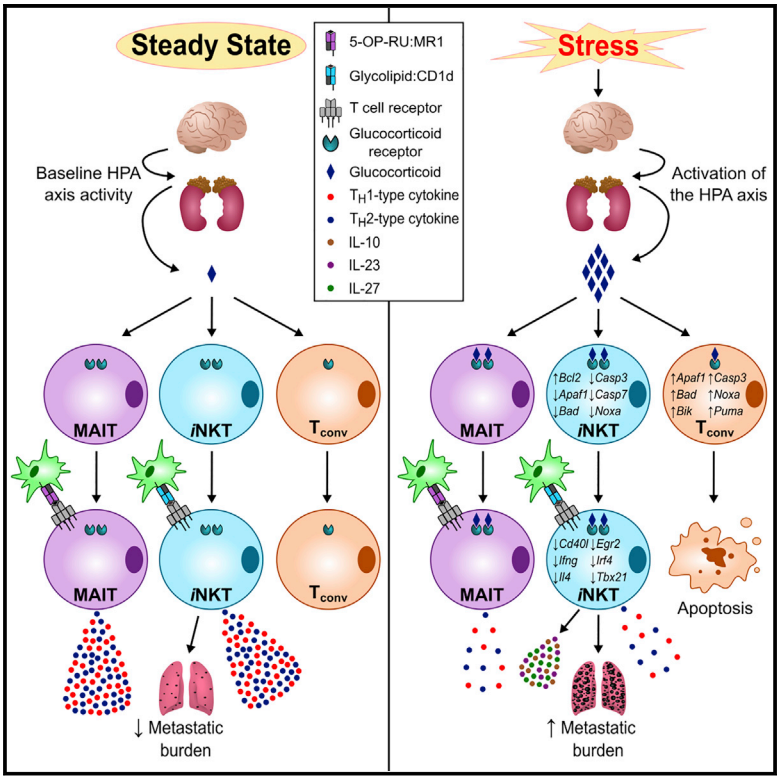

Highlights

- *i*T cells are unusually refractory to stress- and glucocorticoid-induced apoptosis
- Chronic stress curbs both T_H1- and T_H2-type responses orchestrated by *i*T cells
- Stress incapacitates *i*NKT cells via intrinsic glucocorticoid receptor signaling
- Stress-elicited glucocorticoids impair the antitumor activity of *i*NKT cells

Authors

Patrick T. Rudak, Joshua Choi, Katie M. Parkins, ..., Wataru Inoue, Olivier Lantz, S.M. Mansour Haeryfar

Correspondence

mansour.haeryfar@schulich.uwo.ca

In brief

Invariant T cells are emergency responders to infection and cancer. Rudak et al. report that psychological stress unusually spares these innate-like T lymphocytes but alters or impairs their cytokine production and cytotoxic and/or antimetastatic capacities through a cell-autonomous, glucocorticoid receptor-dependent mechanism. This may explain certain aspects of stress-induced immunosuppression.

Rudak et al., 2021, Cell Reports *35*, 108979
April 13, 2021
https://doi.org/10.1016/j.celrep.2021.108979

CellPress

Cell Reports

CellPress
OPEN ACCESS

Article

Chronic stress physically spares but functionally impairs innate-like invariant T cells

Patrick T. Rudak,[1] Joshua Choi,[1] Katie M. Parkins,[2,3] Kelly L. Summers,[1] Dwayne N. Jackson,[2] Paula J. Foster,[2,3] Anton I. Skaro,[4] Ken Leslie,[4] Vivian C. McAlister,[4] Vijay K. Kuchroo,[5] Wataru Inoue,[3,6] Olivier Lantz,[7] and S.M. Mansour Haeryfar[1,4,8,9,*]

[1]Department of Microbiology and Immunology, Western University, London, ON N6A 5C1, Canada
[2]Department of Medical Biophysics, Western University, London, ON N6A 5C1, Canada
[3]Robarts Research Institute, Western University, London, ON N6A 5B7, Canada
[4]Department of Surgery, Division of General Surgery, Western University, London, ON N6A 4V2, Canada
[5]Evergrande Center for Immunologic Diseases, Harvard Medical School and Brigham and Women's Hospital, Boston, MA 02115, USA
[6]Department of Physiology and Pharmacology, Western University, London, ON N6A 5C1, Canada
[7]Laboratoire d'Immunologie and INSERM U932, PSL University, Institut Curie, 75248 Paris Cedex 5, France
[8]Department of Medicine, Division of Clinical Immunology and Allergy, Western University, London, ON N6A 5A5, Canada
[9]Lead contact
*Correspondence: mansour.haeryfar@schulich.uwo.ca
https://doi.org/10.1016/j.celrep.2021.108979

SUMMARY

The deleterious effects of psychological stress on mainstream T lymphocytes are well documented. However, how stress impacts innate-like T cells is unclear. We report that long-term stress surprisingly abrogates both T helper 1 (T_H1)- and T_H2-type responses orchestrated by invariant natural killer T (*i*NKT) cells. This is not due to *i*NKT cell death because these cells are unusually refractory to stress-inflicted apoptosis. Activated *i*NKT cells in stressed mice exhibit a "split" inflammatory signature and trigger sudden serum interleukin-10 (IL-10), IL-23, and IL-27 spikes. *i*NKT cell dysregulation is mediated by cell-autonomous glucocorticoid receptor signaling and corrected upon habituation to predictable stressors. Importantly, under stress, *i*NKT cells fail to potentiate cytotoxicity against lymphoma or to reduce the burden of metastatic melanoma. Finally, stress physically spares mouse mucosa-associated invariant T (MAIT) cells but hinders their T_H1-/T_H2-type responses. The above findings are corroborated in human peripheral blood and hepatic *i*NKT/MAIT cell cultures. Our work uncovers a mechanism of stress-induced immunosuppression.

INTRODUCTION

Long-term stress due to persistent negative emotions or repeated exposure to environmental stressors carries adverse immunological consequences (Glaser and Kiecolt-Glaser, 2005). Individuals experiencing greater relative levels of perceived stress mount weaker responses to vaccination and infection (Glaser and Kiecolt-Glaser, 2005). Stress has also been linked to cancer progression in animal models, often implicating diminished or dysregulated antitumor immunity (Kamiya et al., 2019; Kokolus et al., 2013; Partecke et al., 2016; Saul et al., 2005; Yang et al., 2019). According to prospective epidemiological studies, a higher degree of stress is associated with elevated incidences of neoplasia and cancer mortality in previously healthy individuals, and with poorer prognosis in cancer patients (Batty et al., 2017; Chida et al., 2008). Despite such findings, the mechanisms underlying stress-induced immunosuppression are ill defined.

A stress response is typically launched via the coordinated activation of the sympathetic nervous system (SNS) and the hypothalamic-pituitary-adrenal (HPA) axis (Glaser and Kiecolt-Glaser, 2005). Dense innervation of various organs by the SNS, including lymphoid tissues, enables targeted release of specific neurotransmitters into the extracellular milieu in which immune cells operate (Elenkov et al., 2000). Norepinephrine (NE), the most dominant neurotransmitter utilized by post-ganglionic sympathetic nerve termini, signals through α- and/or β-adrenergic receptors (Elenkov et al., 2000). Under profound sympathetic stimulation, NE is co-transmitted from large intraneuronal storage vesicles with neuropeptide Y (NPY) (Straub et al., 2000), which utilizes Y1, Y2, Y4, Y5, and Y6 receptors (Prod'homme et al., 2006). The activation of the HPA axis raises the circulating levels of glucocorticoids, which exert broad anti-inflammatory effects by binding to the glucocorticoid receptor (GR) encoded by *Nr3c1* (Cain and Cidlowski, 2017). Stress-elicited defects in antimicrobial and antitumor immunity are often attributable to the operation of the SNS and/or the HPA axis (Pruett, 2003).

Previous studies on stress and immunity have focused heavily on conventional T (T_{conv}) cells (Calcagni and Elenkov, 2006). By inducing apoptosis in $CD4^+CD8^+$ thymocytes and mature T_{conv}

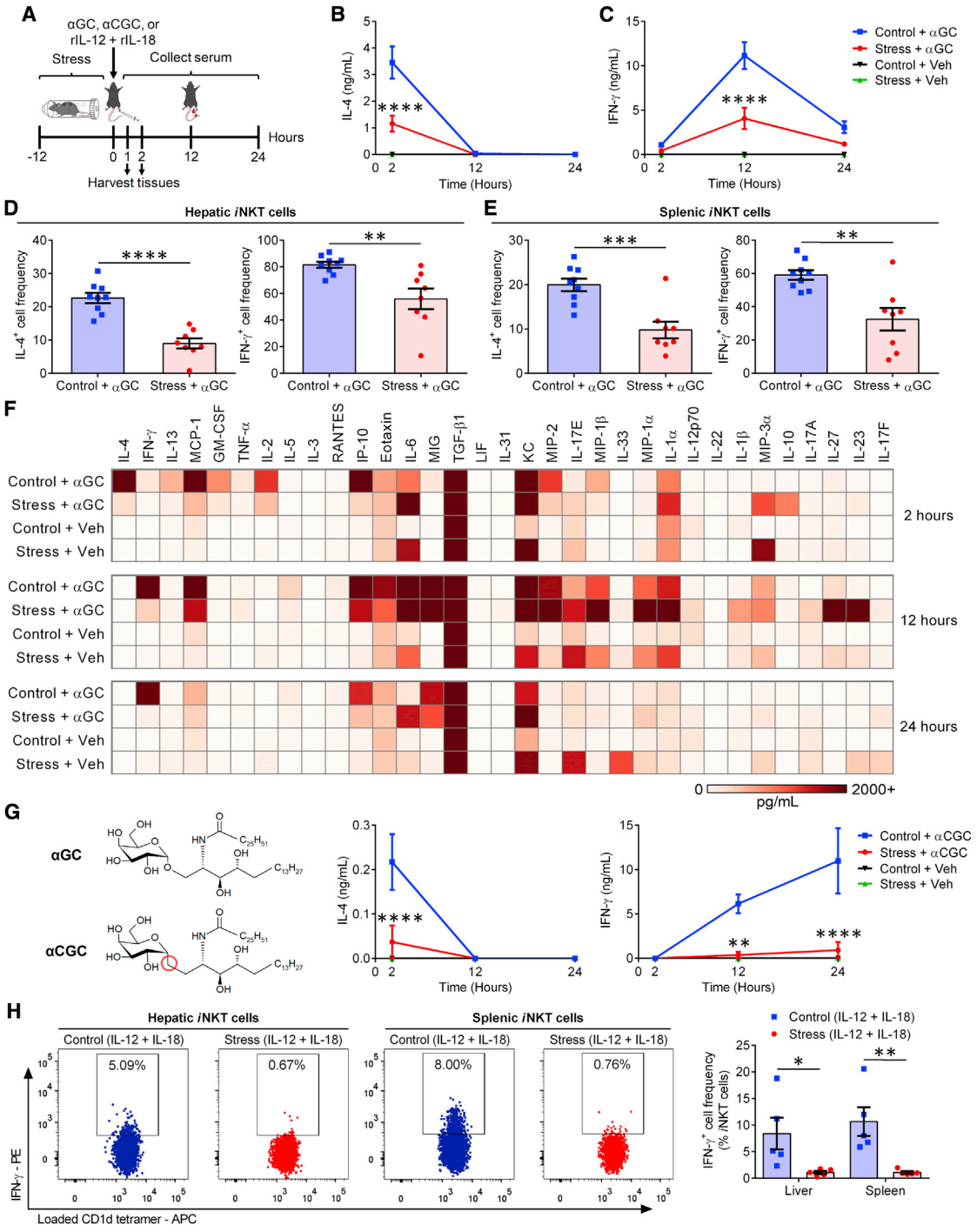

Figure 1. Prolonged stress impairs *i*NKT cells' capacity to trigger IL-4 and IFN-γ production and potentiates an abnormal inflammatory response to glycolipid Ags

(A) WT B6 mice were restrained for 12 h. Control animals remained undisturbed but were deprived of food and water. Mice subsequently received αGC, αCGC, or vehicle (Veh) i.p., or a combination of IL-12 and IL-18 i.v.

(B and C) At the indicated time points post-αGC injection, serum IL-4 (B) and IFN-γ (C) were quantified by ELISA (n = 10 per group).

(D and E) Two hours after αGC injection, IL-4$^+$ and IFN-γ$^+$ cell frequencies among hepatic (D) and splenic (E) TCRβ$^+$PBS-57-loaded CD1d tetramer$^+$ *i*NKT cells were determined by flow cytometry.

(F) Two, 12, and 24 h after αGC (or Veh) administration, serum cytokine levels were measured via multiplex assays, and average values (n = 3 per cohort) were used to generate a heatmap.

(legend continued on next page)

cells, glucocorticoids shrink the size of T cell pools (Haeryfar and Berczi, 2001; Herold et al., 2006). Moreover, stress creates T helper 2 (T_H2) bias (Calcagni and Elenkov, 2006), for instance by favoring interleukin-4 (IL-4) production in the context of *ex vivo* T_{conv} cell stimulation (Hu et al., 2014) or within tumor microenvironments (TMEs) (Hou et al., 2013). NE (Elenkov et al., 2000), NPY (Buttari et al., 2014), and glucocorticoids (Taves and Ashwell, 2020) have each been reported to permit or promote T_H2-skewed phenotypes while inhibiting T_H1-type responses.

To date, how psychological stress affects innate-like invariant T (*i*T) cells, including invariant natural killer T (*i*NKT) and mucosa-associated invariant T (MAIT) cells, has not been explored. This is a critical question given the remarkable immunomodulatory, cytotoxic, antitumor, antibacterial, and antiviral properties of these cells (Haeryfar and Mallevaey, 2015; Haeryfar et al., 2018; Lisbonne et al., 2004; Rudak et al., 2018; Zhang et al., 2019).

*i*NKT cells bear a CD1d-restricted, glycolipid-reactive, semi-invariant T cell receptor (*i*TCR), which contains a canonically rearranged α chain (Vα14-Jα18 in mice and Vα24-Jα18 in humans) paired with one of only few Vβ chain choices (Lantz and Bendelac, 1994). Activated *i*NKT cells swiftly produce copious quantities of T_H1, T_H2, and/or T_H17 cytokines that shape ensuing immune responses (Matsuda et al., 2008). The prototypic glycolipid ligand of *i*NKT cells, α-galactosylceramide (αGC) (Kawano et al., 1997), prompts the transactivation of several effector cell types, including NK cells (Smyth et al., 2002), precursors to mature NK (pre-mNK) cells (Choi et al., 2019), and $CD8^+$ T_{conv} cells (Nakagawa et al., 2004). Therefore, αGC and its analogs are pursued as potential therapeutics (Fujii and Shimizu, 2019; Matsuda et al., 2008).

MAIT cells too harbor *i*TCR α chains (typically Vα19-Jα33 in mice and Vα7.2-Jα33 in humans) and minimal Vβ chain diversity (Lepore et al., 2014; Rahimpour et al., 2015). They are abundant in human peripheral blood (PB) and strategically poised in the human liver, lungs, and mucosal layers (Dusseaux et al., 2011; Franciszkiewicz et al., 2016; Tang et al., 2013), the ports of entry for many pathogens and common sites of neoplastic transformation or metastatic growth. Upon stimulation with vitamin B intermediates of bacterial and fungal origin (e.g., 5-[2-oxopropylideneamino]-6-D-ribitylaminouracil; 5-OP-RU) (Corbett et al., 2014), certain drugs and drug-like metabolites (Keller et al., 2017; Kjer-Nielsen et al., 2012), and other compounds presented by major histocompatibility complex (MHC)-related protein 1 (MR1), MAIT cells quickly produce a wide array of inflammatory mediators, including T_H1-, T_H2-, and T_H17-type cytokines (Kelly et al., 2019; Kurioka et al., 2017), and transactivate key downstream effectors (Salio et al., 2017). Although best known for their antimicrobial activities, MAIT cells may also play significant roles in various TMEs (Haeryfar et al., 2018; Yao et al., 2020). Both *i*NKT and MAIT cells can also respond to viral infections in a TCR-independent fashion, primarily through cytokines such as IL-12 and IL-18 (Tyznik et al., 2008; van Wilgenburg et al., 2016).

Here, we leveraged multiple mouse models of psychological stress as well as human cell culture systems to investigate the impact of stress on *i*T cell functions.

RESULTS

Psychological stress impairs the ability of *i*NKT cells to trigger IL-4 and IFN-γ production and forces them to promote an atypical systemic inflammatory signature

*i*NKT cells are unconventional, innate-like T cells with emergency response roles in antitumor and antimicrobial immunity (Fujii and Shimizu, 2019); yet, how stress shapes *i*NKT cell responses has been largely unknown.

We compared wild-type (WT) C57BL/6 (B6) mice that were left undisturbed or subjected to prolonged physical restraint (Figure 1A) for their *in vivo* IL-4 and interferon-γ (IFN-γ) responses to αGC (Figures 1A–1C). The primary source of IL-4 in response to this glycolipid are *i*NKT cells—hence, the rapidity with which they release this cytokine (Crowe et al., 2003). To our surprise, confinement stress resulted in dramatically reduced IL-4 levels (Figure 1B), which goes against the T_H2 paradigm of stress and immunity (Calcagni and Elenkov, 2006; Hou et al., 2013; Hu et al., 2014). Peak IFN-γ levels were also similarly decreased in stressed animals (Figure 1C).

*i*NKT cells are not the only source of serum IFN-γ, which is also secreted by secondary effectors such as NK cells after αGC administration (Hayakawa et al., 2001; Smyth et al., 2002). To assess the impact of stress on IFN-γ production by *i*NKT cells, hepatic (Figure 1D) and splenic (Figure 1E) *i*NKT cells were identified via CD1d tetramer staining and examined for their intracellular cytokine content 2 h after αGC treatment. Consistent with serum cytokine results, far fewer *i*NKT cells from stressed mice generated IL-4 or IFN-γ (Figures 1D, 1E, and S1A). Furthermore, purified hepatic *i*NKT cells, which were sorted after restraint stress and exposed to αGC in co-cultures with $CD11c^+$ bone-marrow-derived dendritic cells (BMDCs), were weak cytokine producers (Figure S1B). In contrast, upon *ex vivo* stimulation with phorbol 12-myristate 13-acetate (PMA) and ionomycin, *i*NKT cells from stressed animals demonstrated intact IL-4 and IFN-γ production capacities (Figure S1C). PMA and ionomycin work synergistically to activate protein kinase C and Ca^{2+}/calmodulin-dependent kinases, resulting in T cell activation independently of TCR engagement (Chatila et al., 1989). Therefore, under stress, poor *i*NKT cell responses to cognate antigens (Ags) are likely due to impaired *i*TCR-proximal signaling events. We found splenic *i*NKT cells from stressed animals to express reduced levels of *i*TCR αβ, CD28, and inducible T cell costimulator (ICOS) (Figure S1D). These changes were accompanied by decreased phospho-SLP76 (pY128) levels and a trend toward diminished phospho-CD3ζ (pY142) and phospho-ZAP70 (pY319)/phospho-Syk (pY352) levels, but not phospho-Lck (pY505), in hepatic *i*NKT cells (data not shown).

(G) Separate cohorts (n = 4) were injected with αCGC or Veh, and blood IL-4 and IFN-γ levels were measured by ELISA.
(H) Parallel cohorts received IL-12 and IL-18 and were sacrificed 1 h later for their livers and spleens, in which $IFN\text{-}\gamma^+$ *i*NKT cell percentages were determined. Each symbol in (D), (E), and (H) represents an individual mouse. Error bars represent SEM. *, **, ***, and **** denote differences with $p < 0.05$, $p < 0.01$, $p < 0.001$, and $p < 0.0001$, respectively, by two-way ANOVA with Dunnett's correction (B, C, and G) or unpaired Student's t tests (D, E, and H).

Intrinsic host factors dictate or contribute to skewed cytokine responses in genetically diverse mammals. For instance, B6 and BALB/c mice are considered T_H1- and T_H2-dominant animals, respectively (Mills et al., 2000; Watanabe et al., 2004). Previous reports have suggested differences between these strains in terms of susceptibility to stress (Flint and Tinkle, 2001). However, similar to B6 mice, BALB/c mice that had been stressed before receiving αGC had lower blood IL-4 and IFN-γ levels (Figure S2A).

There is sexual dimorphism in sensitivity to various stressors (Buynitsky and Mostofsky, 2009). In addition, *i*NKT cell frequencies and cytokine profiles, including IL-4 and IFN-γ responses to αGC, may differ between males and females (Bernin et al., 2016; Gourdy et al., 2005). We found restraint stress to similarly reduce serum IL-4 and IFN-γ concentrations in both sexes (Figure S2B).

IL-4 and IFN-γ are classic T_H2 and T_H1 cytokines, respectively. However, numerous other cytokines and chemokines also participate in inflammatory processes. To more widely capture the *i*NKT cell response landscape amid prolonged stress, we performed multiplex analysis on serum samples collected 2, 12, and 24 h after treatment with αGC or vehicle. A multitude of cytokines, other than IL-4 and IFN-γ, were significantly reduced at one or several time points in the serum of stressed mice. These included IL-2, IL-5, IL-13, eotaxin, granulocyte-macrophage colony-stimulating factor (GM-CSF), IFN-γ-inducible protein 10 (IP-10)/CXCL10, monocyte chemoattractant protein-1 (MCP-1)/CCL2, RANTES/CCL5, and tumor necrosis factor α (TNF-α) (Figures 1F and S3). In our cytofluorimetric analyses, we confirmed diminished intracellular levels of IL-2, IL-5, and IL-13 in αGC-stimulated *i*NKT cells from stressed animals (Figures S1E–S1G). In contrast with the above mediators, IL-10, IL-23, and IL-27 became notably detectable at strikingly high quantities in animals that had been restrained (Figures 1F and S3). Furthermore, stress augmented the production of IL-1α, IL-1β, macrophage inflammatory protein-1α (MIP-1α)/CCL3, and MIP-3α/CCL20 in αGC-treated mice (Figures 1F and S3) and also resulted in a trend toward increased IL-17A levels at the 12-h time point ($p = 0.075$).

There were a number of cytokines whose serum levels were not different between stressed and control cohorts, including granulocyte colony-stimulating factor (G-CSF), IL-6, IL-7, IL-9, IL-15, IL-17E/IL-25, IL-17F, IL-21, IL-22, IL-28B/IFNL3, IL-31, IL-33, keratinocyte-derived chemokine (KC)/CXCL1, leukemia inhibitory factor (LIF), lipopolysaccharide-inducible CXC chemokine (LIX)/CXCL5, macrophage colony-stimulating factor (M-CSF), monokine induced by IFN-γ (MIG)/CXCL9, MIP-1β/CCL4, MIP-2/CXCL2, transforming growth factor β1 (TGF-β1), TGF-β2, TGF-β3, and vascular endothelial growth factor (VEGF) (Figure 1F and data not shown).

Taken together, our cytokine analyses indicate that *i*NKT cells defy the popular belief that stress indiscriminately steers all T cell responses toward a purely or heavily T_H2-biased phenotype. Instead, *i*NKT cells display a mixed signature dominated by "select" pro- and anti-inflammatory cytokines. Even within the same general category, atypical patterns emerged. For example, whereas stress raised the levels of IL-1α and IL-1β after αGC injection, TNF-α was diminished and IL-6 remained unaltered.

Our multiplexing analyses did not include a 6-h time point post-αGC administration, at which IL-12 reaches its peak levels (Fujii et al., 2002). This was remedied in separate ELISAs in which a nearly 10-fold reduction in IL-12 was evident. To be exact, serum IL-12 levels were 4,355 ± 422 pg/mL and 403 ± 278 pg/mL in control and stressed animals, respectively. Given the prominent role of DCs in IL-12 production following *in vivo* *i*NKT cell activation (Blumenfeld et al., 2011; Fujii et al., 2006), we examined the frequency of IL-12$^+$ DCs, which was significantly reduced in stressed mice that had received αGC 6 h earlier (Figure S1H). The above results are consistent with a "split mini-signature" even among classic pro-inflammatory cytokines.

Next, we determined whether stress alters *i*NKT cell responses to CD1d-binding glycolipids other than αGC. We found prolonged restraint (Figure 1A) to suppress cytokine responses triggered by α-C-galactosylceramide (αCGC), a T_H1-polarizing analog of αGC that carries a single glycosidic O-to-CH_2 substitution (Figure 1G) (Schmieg et al., 2003). To ascertain whether stress compromises CD1d/*i*TCR-independent, cytokine-driven *i*NKT cell responses, we used a combination of IL-12 and IL-18, which enables NK cells and innate-like T cells to produce IFN-γ (Velázquez et al., 2008). Therefore, we subjected mice to restraint before injecting them with IL-12 and IL-18 (Figure 1A). Both hepatic and splenic *i*NKT cells from stressed mice failed to produce IFN-γ in this setting (Figure 1H). Similarly, NK cells from a stressed cohort were unable to mount an optimal IFN-γ response to IL-12 and IL-18 (Figure S1I).

Collectively, prolonged psychological stress abrogates IL-4 and IFN-γ responses that are either elicited or potentiated by αGC-exposed *i*NKT cells. This finding appears reproducible across different genetic backgrounds in both sexes and irrespective of *i*NKT cells' tissue location and activation mode. The mixed inflammatory signature observed in stressed animals represents a stark contrast with T_H2-polarized T_{conv} responses.

Unlike other lymphocyte subsets, *i*NKT cells are refractory to stress- and glucocorticoid-induced apoptosis

Mediators of stress disrupt certain defense mechanisms by inducing apoptosis in lymphocytes (Herold et al., 2006; Tseng et al., 2005; Yin et al., 2000). As expected, non-parenchymal hepatic mononuclear cell (HMNC) and splenocyte counts were significantly lower in stressed mice than in controls immediately after restraint ($2.2 \times 10^6 \pm 0.2 \times 10^6$ versus $3.5 \times 10^6 \pm 0.3 \times 10^6$ for HMNCs; $54.7 \times 10^6 \pm 7.8 \times 10^6$ versus $77.6 \times 10^6 \pm 6.3 \times 10^6$ for splenocytes; n = 6 per group) and also 2 h after αGC administration ($1.2 \times 10^6 \pm 0.1 \times 10^6$ versus $2.3 \times 10^6 \pm 0.1 \times 10^6$ for HMNCs; $33.2 \times 10^6 \pm 7.0 \times 10^6$ versus $62.0 \times 10^6 \pm 8.3 \times 10^6$ for splenocytes; n = 5 per group). Therefore, because physical restraint impeded IL-4 and IFN-γ responses to αGC (Figure 1), we asked whether cytokine-producing cells had simply died. We found increases, rather than decreases, in hepatic and splenic *i*NKT cell frequencies in stressed mice (Figure 2A). This was curious because Ki67$^+$ *i*NKT cell frequencies were similar between stressed and control animals (30.3% ± 6.7% versus 27.0% ± 3.0% for hepatic *i*NKT cells; 17.6% ± 3.3% versus 21.7% ± 5.3% for splenic *i*NKT cells; n = 4 per group), dismissing the possibility that *i*NKT cells had undergone expeditious proliferation during stress. Our finding

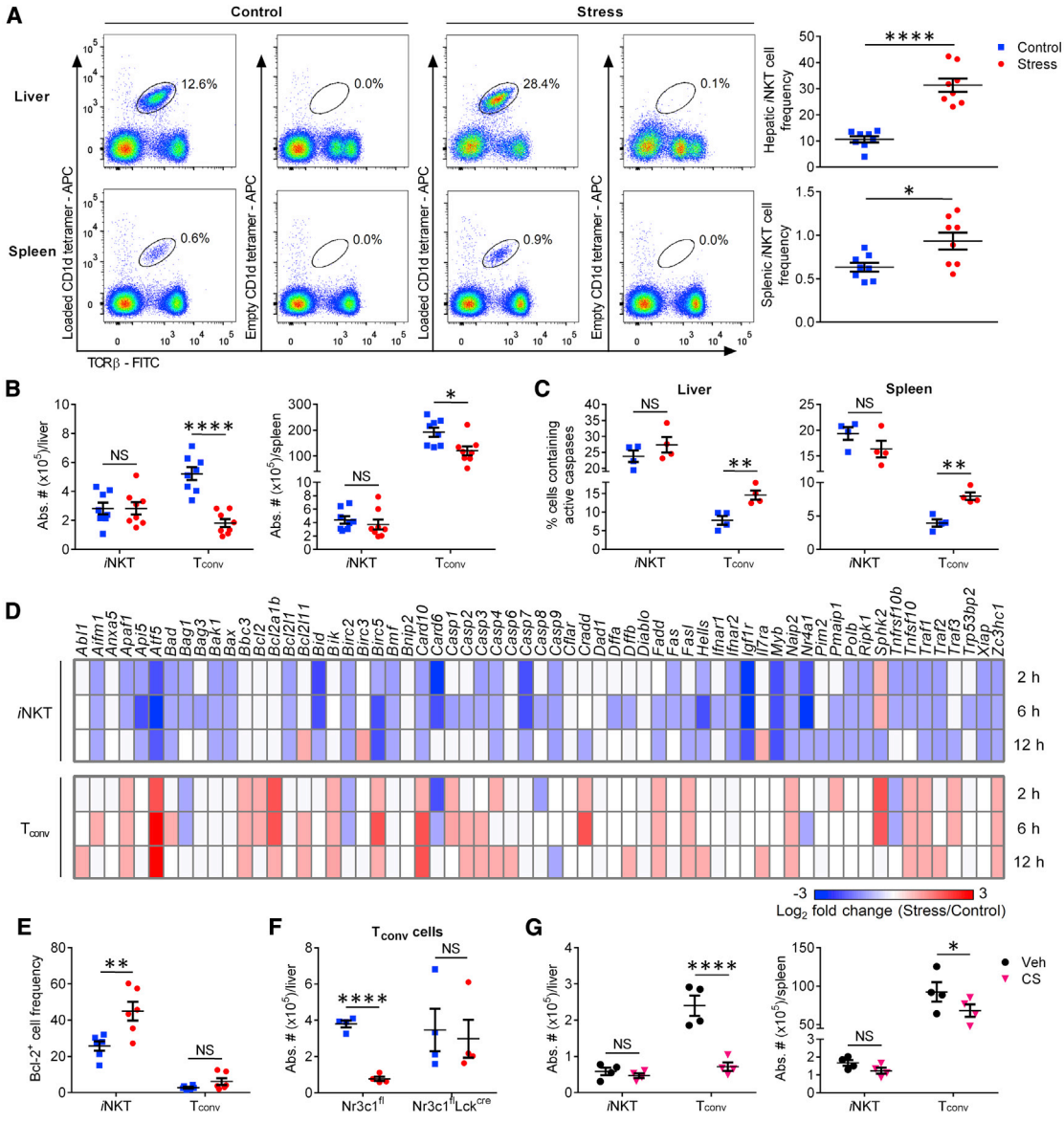

Figure 2. Unlike T_{conv} cells, *i*NKT cells are resistant to glucocorticoid-induced apoptosis

(A) WT B6 mice were left undisturbed or restrained for 12 h, after which HMNCs and splenocytes were harvested and stained with a monoclonal antibody (mAb) to TCRβ along with empty (control) or PBS-57-loaded CD1d tetramers. Representative dot plots and summary data depict hepatic and splenic *i*NKT cell frequencies in stressed and control mice.

(B) The absolute numbers of *i*NKT and TCRβ$^+$PBS-57-loaded CD1d tetramer$^-$ T_{conv} cells were also calculated.

(C) In addition, the percentages of *i*NKT and T_{conv} cells containing active caspases were determined by flow cytometry.

(D) Hepatic *i*NKT and T_{conv} cells were purified from ≥5 mice that had been either subjected to 2, 6, or 12 h of restraint stress or left undisturbed. After obtaining cDNA, the indicated gene products were amplified by quantitative PCR. Gene expression fold changes in *i*NKT and T_{conv} cells isolated from stressed mice relative to corresponding cell populations from control animals were calculated using the $2^{-(\Delta\Delta Ct)}$ method and used to generate a heatmap.

(E) Hepatic *i*NKT and T_{conv} cells were analyzed for their intracellular Bcl-2 content.

(F) Hepatic T_{conv} cells were enumerated in Nr3c1^{fl} and Nr3c1^{fl}Lck^{cre} mice that had been either restrained or left undisturbed.

(G) Cohorts of WT B6 mice were given corticosterone (CS) or Veh in drinking water for 21 days before they were sacrificed for their livers and spleens, in which *i*NKT and T_{conv} cells were enumerated.

Each symbol in (A)–(C) and (E)–(G) represents an individual mouse, and error bars represent SEM. *p < 0.05, **p < 0.01, ****p < 0.0001 by unpaired Student's t tests. NS, not significant.

that *i*NKT cells' absolute numbers remained stable in contrast with marked drops in T_{conv} cell numbers (Figure 2B) suggested that *i*NKT cells were insensitive to stress-provoked apoptosis. This was validated by measuring the intracellular active caspase content of these cells (Figure 2C).

*i*NKT cells are "pre-activated, memory-like" T cells (D'Andrea et al., 2000; Park et al., 2000). Therefore, we asked whether their resistance to apoptosis was a mere reflection of this feature and thus mimicable by the memory subset of T_{conv} cells. Naive and memory T_{conv} pools were distinguished based on CD44 expression (Figure S4A). Similar to unfractionated and naive T_{conv} cells, and unlike *i*NKT cells, $CD44^+$ memory T_{conv} cells were less frequent and contained more active caspases in restrained animals (Figure S4B). Therefore, *i*NKT cells' resistance to stress is not linked to their memory-like property.

To shed light on the molecular mediators of cell survival and death in our system, we analyzed the transcript levels of relevant genes in sorted cells 2, 6, and 12 h into restraint stress. Compared with baseline levels, several pro-apoptotic genes were upregulated in T_{conv} but not in *i*NKT cells. These included the apoptosome component *Apaf1*, the Bcl-2 family members *Bad*, *Bbc3*, *Bik*, and *Pmaip1*, and the executioner caspases-*3* and -*6* (Figure 2D). In fact, a number of these genes were downregulated in *i*NKT cells. At the protein level, the pro-survival molecule Bcl-2 was elevated in *i*NKT cells, but not in the remaining T_{conv} cells (Figure 2E). Therefore, Bcl-2 may have a preventative or compensatory role in circumventing the apoptogenic effects of stress on *i*NKT cells.

Glucocorticoids are culprits of T cell apoptosis under certain circumstances (Haeryfar and Berczi, 2001; Herold et al., 2006). As such, we posited that the dimorphic impact of stress on *i*NKT and T_{conv} cells stems from differential glucocorticoid actions in these cell types. To this end, we generated mice whose T cells were devoid of GR. Indeed, restraint stress reduced T_{conv} cell numbers in B6.Nr3c1$^{fl/fl}$ (Nr3c1^{fl}) controls but not in B6.Nr3c1$^{fl/fl}$Lck$^{cre/WT}$ (Nr3c1^{fl}Lck^{cre}) mice (Figure 2F). We also observed a sharp numerical decline in hepatic and splenic NK and B cells during prolonged stress, which was reversible by treatment with the GR antagonist RU486 (Figure S4C).

Exogenous glucocorticoids are prescribed for many diseases and conditions. Therefore, we tested the effect of long-term, oral administration of corticosterone (CS), the main glucocorticoid in rodents (Pruett, 2003), on T cell apoptosis. Similar to endogenous glucocorticoids, CS reduced T_{conv}, but not *i*NKT, cell numbers both in the liver and in the spleen (Figure 2G), a finding that also serves to confirm the dominant role of glucocorticoids in stress-induced T_{conv} cell demise.

To summarize, *i*NKT cells' unusual resilience in the face of a stress response is mediated by glucocorticoid-GR interactions. Importantly, the above results also rule out cell death as the reason behind the dwarfed IL-4 and IFN-γ responses of *i*NKT cells to glycolipid Ags or cytokines (Figure 1) in stressed animals.

Stress suppresses αGC-elicited cytokine responses through an *i*NKT cell-intrinsic, GR signaling-dependent mechanism independently of neurotransmission from post-ganglionic sympathetic neurons

We next attempted to elucidate the upstream neurological pathway(s) governing *i*NKT cell hyporesponsiveness in the context of prolonged restraint stress. Given the paramount role of the SNS in the fight-or-flight response (Elenkov et al., 2000), we first looked into the expression of SNS neurotransmitter receptors in *i*NKT cells purified from the liver of treatment-naive B6 mice. We did not detect *Npy1r*, *Npy2r*, *Npy4r*, *Npy5r*, or *Npy6r* transcripts (data not shown), and synthetic NPY failed to modulate cytokine production by the *i*NKT cell hybridoma DN32.D3 in response to αGC (data not shown). Hepatic *i*NKT cells had detectable mRNAs encoding the adrenergic receptors *Adra2a*, *Adra2b*, *Adrb1*, and *Adrb2* at levels comparable to or lower than those found in matched hepatic T_{conv} cells (Figure S5A). In addition, NE inhibited IL-2 production by αGC-stimulated DN32.D3 cells (Figure S5B), which was preventable by β-adrenergic receptor antagonism with propranolol (Figure S5C). However, this was only an *in vitro* event because chemical sympathectomy through 6-hydroxydopamine (OHDA) administration failed to restore IL-4 and IFN-γ production in restrained mice that subsequently received αGC (Figure 3A). Sympathectomy was confirmed by reduced tyrosine hydroxylase (TH) staining in the spleens of OHDA-treated animals (Figure 3B). In these experiments, the brain served as a negative control because OHDA does not cross the blood-brain barrier (Schober, 2004).

We then shifted our focus back onto the HPA axis and glucocorticoids. Elevated serum CS in stressed mice reassured us that prolonged restraint in our hands could induce robust activation of the HPA axis (Figure 3C). We found pretreatment with the glucocorticoid synthesis inhibitor metyrapone to rescue IL-4 and IFN-γ production in stressed mice receiving αGC (Figure 3D). To ensure that our results were not confounded by the reported buildup of circulating 11-deoxycorticosterone upon metyrapone treatment (Cao et al., 2002), we used a second pharmacological approach, namely GR antagonism by RU486. Similar to metyrapone, RU486 could prevent the suppressive effect of stress on cytokine production in restrained animals (Figure 3E). Of note, we used male mice in these experiments out of an abundance of caution to avoid the antagonistic action of RU486 on progesterone receptors (Pruett, 2003).

Although the systemic ablation of GR signaling could relieve *i*NKT cell hyporesponsiveness during stress, it was unclear whether glucocorticoids were acting on *i*NKT cells directly or on other cell types such as glycolipid Ag-presenting cells. We first demonstrated that *i*NKT cells from naive mice express the GR, at a greater level than that in matched T_{conv} cells. This was manifest at both mRNA and protein levels (Figures 4A and 4B). Second, we observed that stress instigates GR signaling in hepatic and splenic *i*NKT cells as judged by increased intracellular levels of the anti-inflammatory protein glucocorticoid-induced leucine zipper (GILZ), a known transcriptional target of the activated GR (Figure 4C) (Bereshchenko et al., 2019). Finally, unlike in the Nr3c1^{fl} control cohort, stress failed to compromise the IFN-γ response of αGC-injected Nr3c1^{fl}Lck^{cre} mice (Figure 4D). This was not due to the possible off-target effects of the Cre recombinase because IFN-γ levels were not rescued in stressed B6.Lck$^{cre/WT}$ (Lck^{cre}) mice (Figure 4E). T_{conv} cells do not contribute to rapid IFN-γ production in αGC-treated animals. Therefore, one may infer that direct GR signaling disrupts the ability of *i*NKT cells to generate or trigger inflammatory cytokine responses *in vivo*.

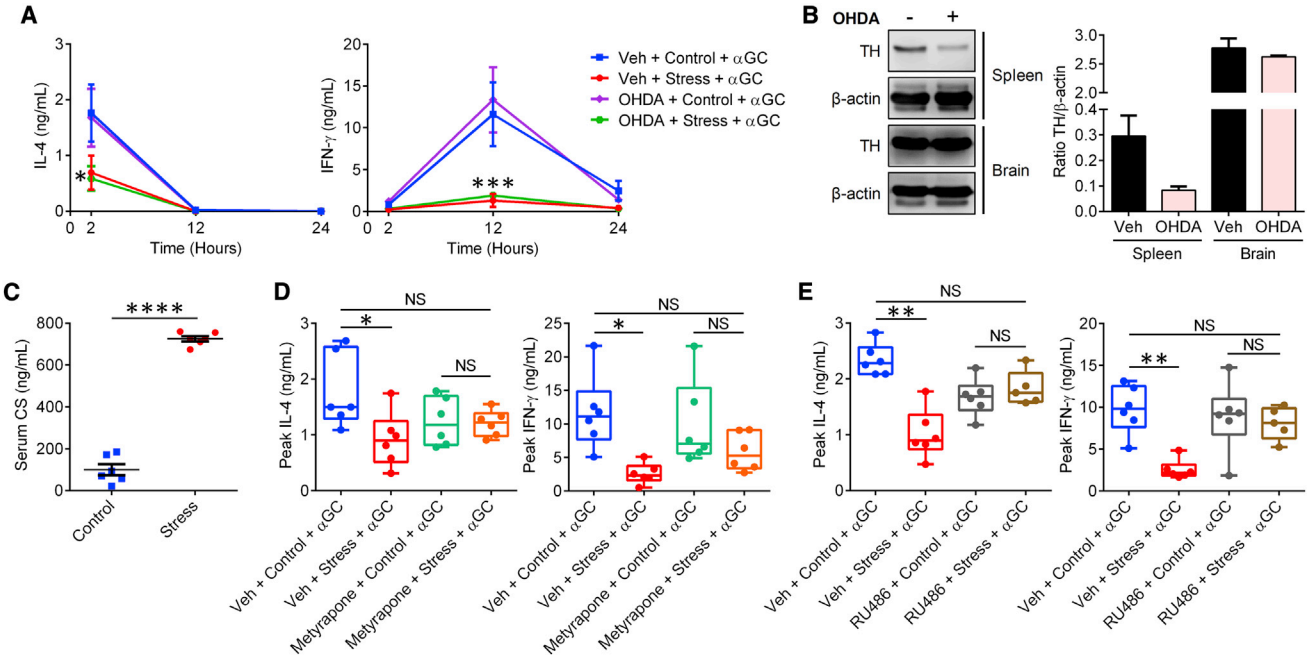

Figure 3. Stress-induced suppression of *i*NKT cell responses is mediated by glucocorticoids, not by SNS signals

(A) WT B6 mice (n = 3 or 4 per group) were injected i.p. with OHDA or Veh 6 days before they were restrained. Control cohorts were left undisturbed. Stressed and control animals were injected with αGC and bled at the indicated time points. Circulating IL-4 and IFN-γ levels were measured by ELISA.

(B) Protein extracts from flash-frozen spleen and brain samples from mice in (A) were loaded onto the same SDS-polyacrylamide gel and examined for their tyrosine hydroxylase (TH) content by western blotting. Staining for β-actin was used to ensure equal protein loading. Summary data illustrate normalized TH levels after densitometry analyses.

(C) Separate cohorts that had been restrained for 12 h or left undisturbed were bled for serum CS quantification by ELISA.

(D and E) Mice were injected i.p. with metyrapone (D) or RU486 (E) 1 h before they were restrained for 12 h (or not) followed by an i.p. injection of αGC. Box-and-whisker plots show IL-4 and IFN-γ levels at 2- and 12-h time points post-αGC administration, respectively, with each symbol representing an individual mouse. Statistical comparisons were made by two-way ANOVA with Dunnett's correction (A), unpaired Student's t test (C), or one-way ANOVA with Tukey's correction (D and E). *p < 0.05, **p < 0.01, ***p < 0.001, ****p < 0.0001; NS, not significant.

Next, we asked whether physical restraint per se alters the activation status of *i*NKT cells. Consistent with their "pre-activated" phenotype (D'Andrea et al., 2000; Park et al., 2000), hepatic and splenic *i*NKT cells expressed high surface levels of CD25, CD44, and CD69 and minimal CD62L in their steady state (Figure 4F). Moreover, confinement stress failed to appreciably change these baseline levels (Figure 4F). Therefore, we took a more comprehensive approach by comparing the transcriptional profiles of purified *i*NKT cells from stressed and control mice. Although stress upregulated *Bcl2* and *CD127* (*Il7ra*), the mRNA levels of a number of genes that support the effector functions of *i*NKT cells were reduced. These include *Cd40l*, *Il18rap*, *Egr2*, *Irf4*, *Nfatc3*, *Tbx21*, *Ifng*, *Il4*, *Gzma*, *Tnf*, *Tnfrsf9*, and *TNFsf10* (Figure 4G). Therefore, wide-ranging *i*NKT cell dysfunctions, beyond select cytokine production, can be expected in the aftermath of stress-induced GR signaling.

Long-term exposure to multiple unpredictable stressors, but not to the same stressor, hinders *i*NKT cell functions

Chronic stress can be due to long-term exposure to different stressful events or elements, resulting in sustained glucocorticoid release in the absence of organismal "habituation." This can be simulated by the chronic variable stress (CVS) model whereby mice are subjected to heterotypic psychological and/or physical stressors, once daily and once nightly, for 21 days (Figure 5A). Given the importance of GR signaling in restraint-induced *i*NKT cell impairments, we hypothesized that CVS should impede *in vivo* cytokine production in response to αGC. We first confirmed elevated blood CS levels at the conclusion of the CVS experiment (Figure 5B), consistent with previous reports that CVS continuously activates the HPA axis (Franco et al., 2016). In addition, hepatic and splenic *i*NKT cells maintained their absolute numbers in mice that had been subjected to CVS (Figure 5C). Finally, and as hypothesized, animals that were injected with αGC after CVS had lower levels of IL-4, IFN-γ, and IL-2 (Figure 5D). We also exposed parallel cohorts of mice repeatedly to the same stressor, physical restraint, for 21 consecutive days before αGC treatment. In this repeated restraint stress (RRS) model, animals predict the stressor and habituate and adapt to it by gradually de-escalating glucocorticoid release (Girotti et al., 2006). Indeed, αGC-induced cytokine production remained impeccable in mice that had undergone RRS (Figure 5D), a sharp contrast with the CVS model.

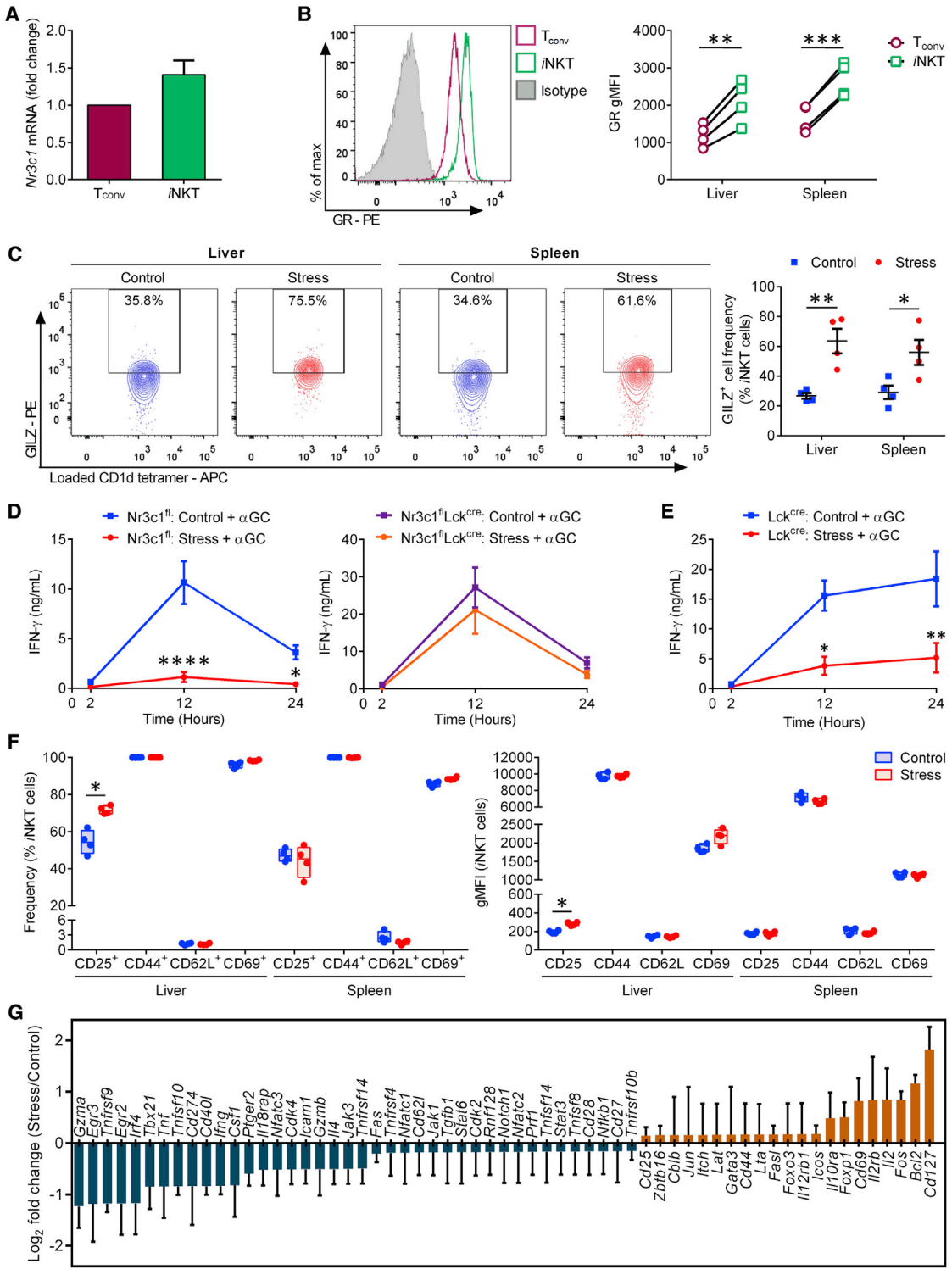

Figure 4. Stress impedes *i*NKT cell responses to αGC in a cell-autonomous, GR-dependent manner and creates a transcriptomic signature consistent with extensive *i*NKT cell dysfunctions

(A) Hepatic *i*NKT and T_{conv} cells from naive B6 mice (n = 10 per experiment) were fluorescence-activated cell sorting (FACS) purified and the *Nr3c1* mRNA content of *i*NKT cells relative to that of T_{conv} cells was PCR quantitated. Fold-change values were determined in 3 independent experiments.

(legend continued on next page)

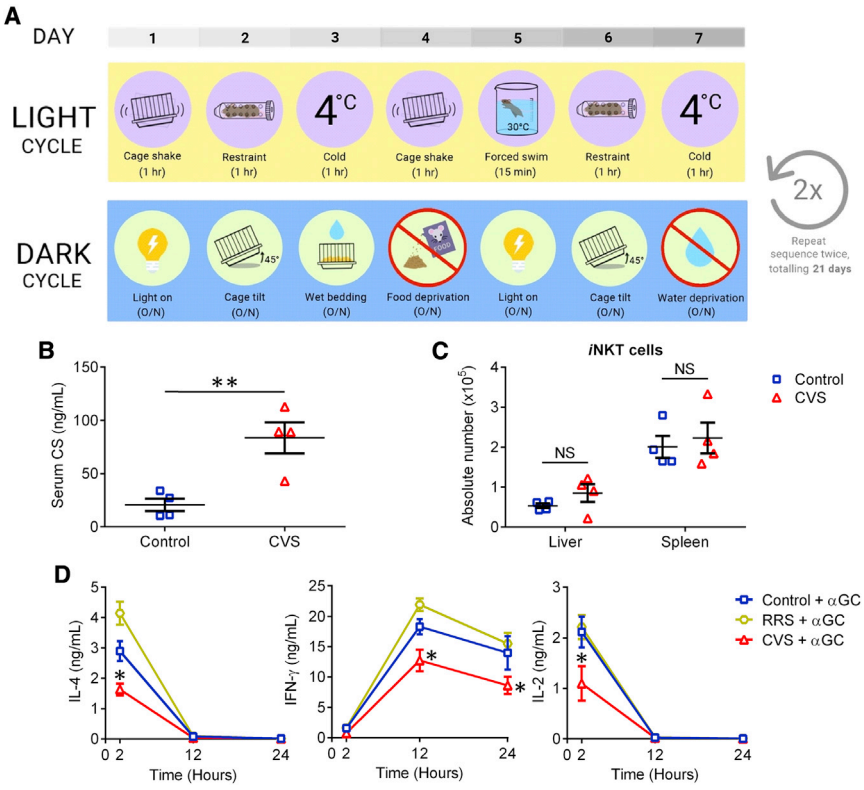

Figure 5. Prolonged exposure to unpredictable stressors impairs cytokine production in response to αGC

(A) B6 mice were subjected to 21 days of chronic variable stress (CVS) involving 3 weekly cycles of exposure to the indicated heterotypic stressors. Control mice remained undisturbed in home cages with food and water supplied *ad libitum*.

(B and C) At the conclusion of the third cycle, serum CS was measured by ELISA (B), and hepatic and splenic *i*NKT cells were enumerated (C).

(D) In additional experiments, parallel cohorts of mice (n = 4 per group) were subjected to CVS, or to repeated restraint stress (RRS) involving 1 h of daily physical confinement for 21 consecutive days. Control mice were left undisturbed. At the conclusion of the 21-day period, animals were injected with αGC and assessed for their serum IL-4, IFN-γ, and IL-2 levels at the indicated time points. Each symbol in (B) and (C) represents a mouse. Error bars denote SEM. Statistical comparisons were conducted using unpaired Student's t tests (B and C) or two-way ANOVA with Tukey's correction (D). *p < 0.05, **p < 0.01; NS, not significant.

The above results further enforce our conclusion that the activation of the HPA axis mediates stress-induced *i*NKT cell dysfunctions.

Glucocorticoid secretion due to prolonged stress interferes with *i*NKT cells' antimetastatic function

*i*NKT cells participate in anticancer immune surveillance, and their glycolipid agonists have been used in clinical trials for multiple malignancies (Fujii and Shimizu, 2019; van den Heuvel et al., 2011). However, whether stress alters the antitumor property of *i*NKT cells has not been addressed.

We first assessed the oncolytic capacity of splenocytes from mice that had been subjected to prolonged restraint before they received an αGC injection. Effector cells isolated from stressed mice were less competent in killing YAC-1 lymphoma cells *in vitro* (Figure 6A). We then used an *in vivo* killing assay with which to test the ability of αGC-transactivated NK cells and pre-mNK cells to destroy B6.β2M$^{-/-}$ (β2M$^{-/-}$) splenocytes (Choi et al., 2019). Consistent with our *in vitro* results, β2M$^{-/-}$ target cells were only poorly cleared in previously restrained animals (Figure 6B).

Next, we examined whether stress interferes with the ability of αGC-primed *i*NKT cells to prevent metastatic cancer *in vivo*. Mice were restrained, or not, before receiving a single intraperitoneal (i.p.) injection of αGC or vehicle, followed shortly by an intravenous (i.v.) inoculum of B16-F10 melanoma cells. Visual enumeration of pulmonary metastases revealed a complete loss of αGC-mediated protection in stressed mice (Figure 6C). This finding was validated by whole-body bioluminescence imaging of tumor-bearing B6 albino mice that showed far greater B16-F10-Red-FLuc (B16-FLuc) tumor burden in their lungs if they were previously restrained (Figure 6D). Furthermore, RU486 treatment before stress reinstated the efficacy of αGC therapy against B16-F10 metastasis (Figure 6E). Therefore, through a GR-dependent pathway, prolonged psychological

(B) HMNCs and splenocytes were stained with an anti-GR mAb or a mouse IgG2aκ isotype control. Open histograms illustrate the GR positivity of hepatic *i*NKT and T_{conv} cells, and the filled histogram corresponds to the staining of TCRβ$^+$ cells with the above isotype control. Summary data depict the geometric mean fluorescence intensity (gMFI) of GR staining.

(C) HMNCs and splenocytes from mice that had been restrained or left undisturbed were stained with an anti-GILZ mAb or a rat IgG2aκ isotype control. Representative contour plots depict GILZ$^+$ *i*NKT cell frequencies, which are summarized in scatterplots.

(D and E) Nr3c1^{fl} and Nr3c1^{fl}Lck^{cre} mice (n = 6–9) (D) and Lck^{cre} mice (n = 4 or 5) (E) were restrained or left undisturbed before they received αGC, and serum IFN-γ was quantitated by ELISA.

(F) HMNCs and splenocytes from stressed and control mice were stained with mAbs against CD25, CD44, CD62L, and CD69 or with appropriate isotype controls. Box-and-whisker plots illustrate the frequencies of *i*NKT cells staining positively for each marker.

(G) Hepatic *i*NKT cells were sorted using FACS from stressed and control B6 mice (n ≥ 5 per group per experiment). Gene expression fold changes were determined by quantitative PCR in 3 independent experiments.

Each symbol in (B), (C), and (F) represents an individual mouse. Error bars in (A), (C)–(E), and (G) represent SEM. *p < 0.05, **p < 0.01, ***p < 0.001, ****p < 0.0001 by paired (B) or unpaired (C and F) Student's t tests or by two-way ANOVA with Sidak's correction (D and E).

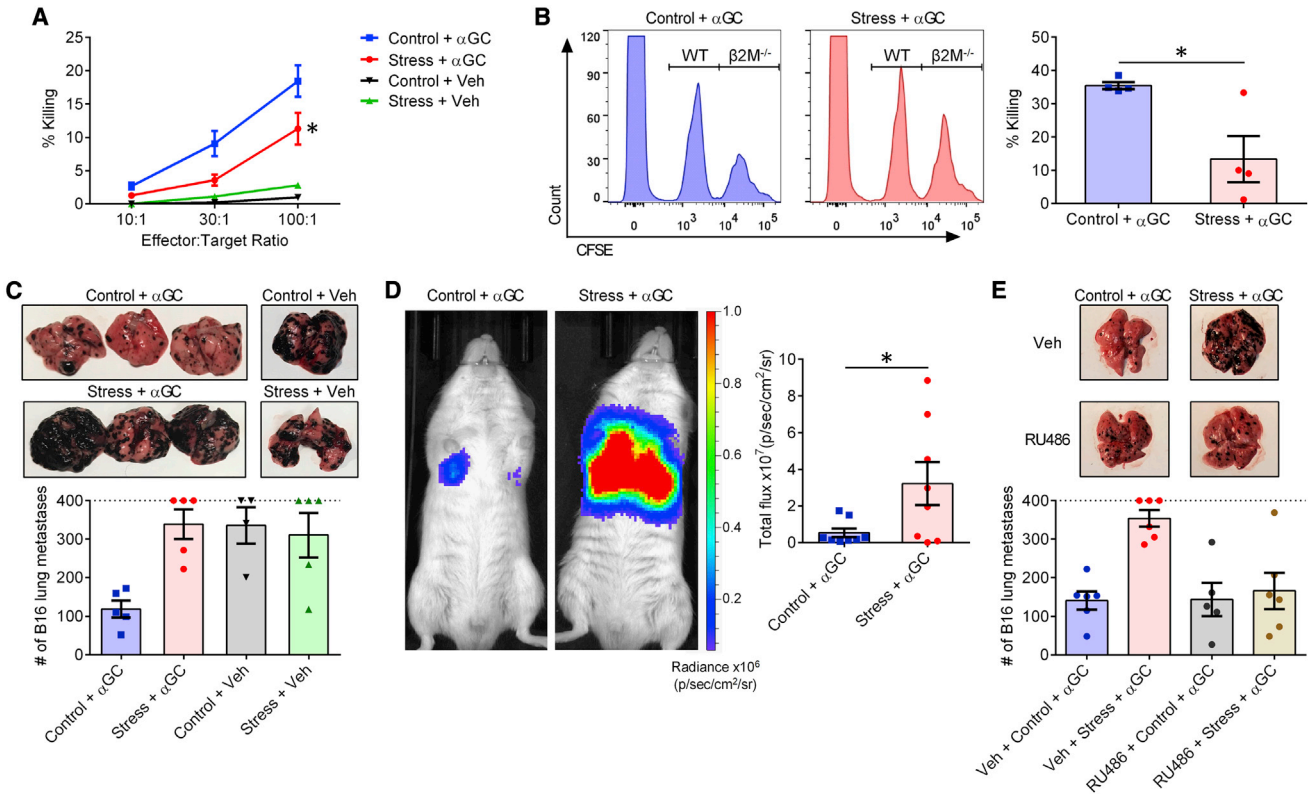

Figure 6. GR signaling during stress compromises the ability of *i*NKT cells to trigger oncolytic and antimetastatic responses

B6 mice were restrained or left undisturbed before they were given αGC (n = 6 or 7) or Veh (n = 2).

(A) Twenty-four hours later, mice were euthanized, and their splenocytes were employed at the indicated effector:target ratios against ^{51}Cr-labeled YAC-1 lymphoma cells. Percent specific cytotoxicity was calculated as described in STAR Methods.

(B) Twenty-four hours after αGC administration, previously stressed and control mice were injected i.v. with a 1:1 mixture of CFSE^{lo} WT B6 and CFSE^{hi} β2M$^{-/-}$ B6 splenocytes. After 2 h, the relative proportion of each population was determined by flow cytometry, and percent cytotoxicity against NK-susceptible β2M$^{-/-}$ target cells was calculated as described in STAR Methods.

(C) In separate experiments, 6 h after αGC (or Veh) administration, mice were injected i.v. with B16-F10 cells. Lungs were photographed 14 days later for representative images, and metastatic lung nodules were visually counted as a measure of tumor burden. Mice bearing too many nodules to count (>400) are conservatively represented on the dotted line.

(D) In similar experiments, B6 albino mice received B16-FLuc cells. Twenty-one days later, they received an i.p. injection of luciferin and were subjected to whole-body bioluminescence imaging.

(E) In additional experiments, B6 mice were used as in (C) except they were injected i.p. with RU486 (or Veh) 1 h before they were restrained (or not).

Each symbol in (B)–(E) represents a mouse. Error bars denote SEM. * denotes a difference with $p < 0.05$ by two-way ANOVA with Tukey's correction (A) or by unpaired Student's t tests (B and D).

stress abolishes the capacity of *i*NKT cells to orchestrate antimetastatic responses.

MAIT cells are resistant to glucocorticoid-induced apoptosis but fail to mount optimal cognate responses under stress

Dubbed "the human cousins" of mouse *i*NKT cells, MAIT cells are MR1-restricted *i*T cells with key roles in host defense (Legoux et al., 2017; Salou et al., 2019). They are scarce in conventional laboratory mice (Cui et al., 2015) but frequent in the human PB, liver, and lungs (Dusseaux et al., 2011; Franciszkiewicz et al., 2016; Tang et al., 2013).

We asked whether similar to mouse *i*NKT cells, human *i*T cells survive exposure to glucocorticoids. We incubated human PB mononuclear cells (PBMCs) (Figure 7A) or HMNCs (Figure 7B) for 24 h with hydrocortisone (HC), the main stress-induced glucocorticoid produced in humans, or with dexamethasone (DEX), a commonly prescribed synthetic glucocorticoid. Exposure to either HC or DEX elevated the intracellular active caspase levels of PB T_{conv} cells (Figure 7A). By contrast, matched blood *i*NKT and MAIT cells contained very low and stable levels of active caspases. A similar pattern was evident among hepatic MAIT cells (Figure 7B). Moreover, in two liver samples in which *i*NKT cells were detectable, there was no evidence of increased caspase activity after incubation with HC or DEX (data not shown).

Similar to mouse *i*NKT and T_{conv} cells from stressed animals, which upregulate CD127 in a cell-autonomous, GR-dependent manner to respond to the pro-survival cytokine IL-7 (Figures S6A–S6E), human MAIT, *i*NKT, and T_{conv} cells increased their

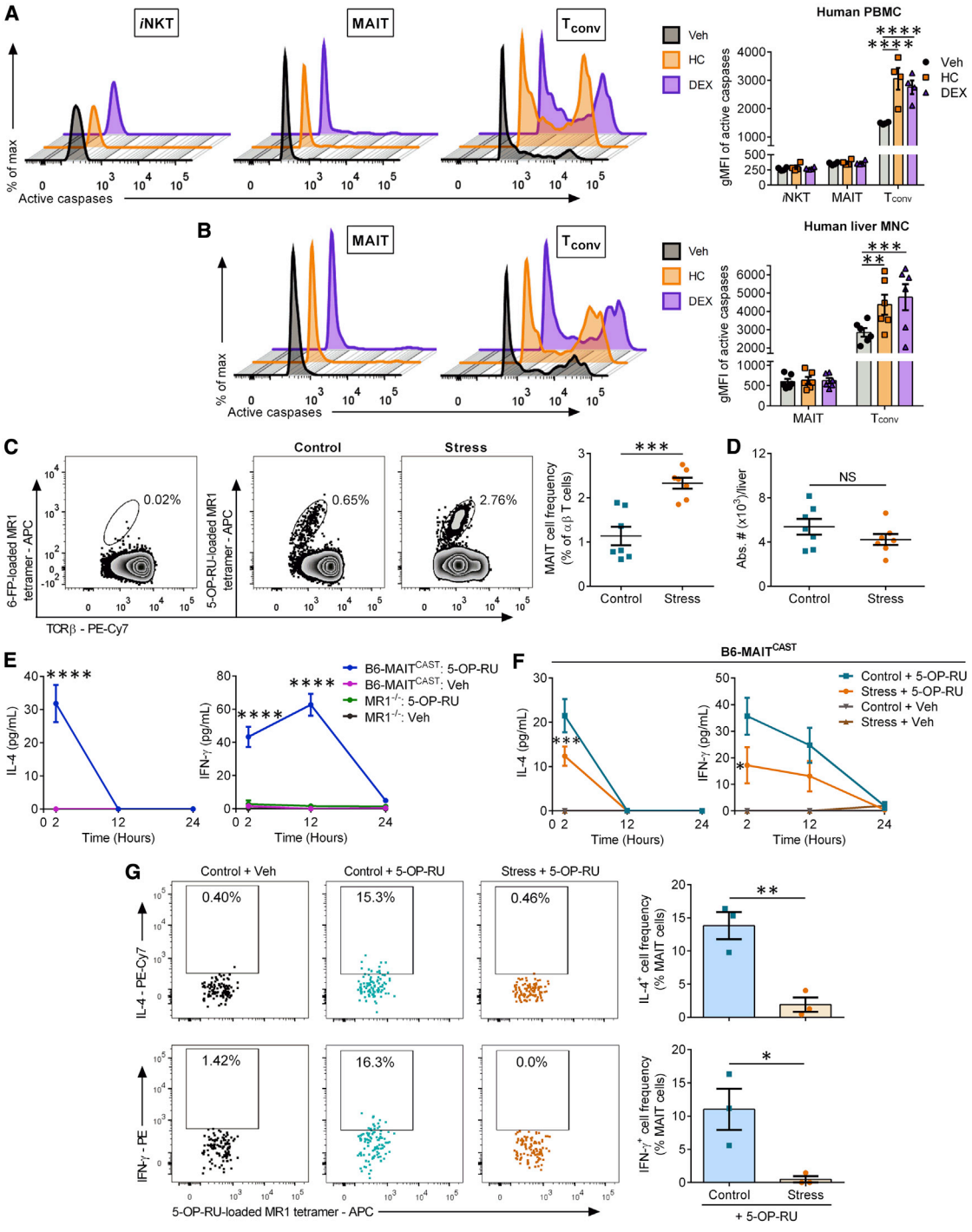

Figure 7. Stress and glucocorticoids fail to program MAIT cells for apoptosis but render them hyporesponsive to 5-OP-RU

(A and B) Human PBMCs (A) and HMNCs (B) were exposed to hydrocortisone (HC), dexamethasone (DEX), or Veh for 24 h before they were analyzed by flow cytometry to detect intracellular active caspases in the indicated T cell subsets. gMFI values are summarized in bar graphs.

(C) Immediately after prolonged restraint stress (or not), HMNCs from B6-MAIT^{CAST} mice were stained with 6-FP- (control) or 5-OP-RU-loaded MR1 tetramers along with anti-TCRβ and -B220 mAbs. Representative zebra plots illustrate MAIT cell populations after gating on TCRβ^{+}B220^{-} events, and scatterplots summarize MAIT cell frequencies among total αβ T cells.

(D) The absolute numbers of hepatic MAIT cells were also calculated.

(E) B6-MAIT^{CAST} and MR1$^{-/-}$ mice ($n \geq 3$) were injected i.p. with 5-OP-RU or Veh, and serum IL-4 and IFN-γ levels were quantified at the indicated time points.

(F) B6-MAIT^{CAST} mice were restrained (or left undisturbed), injected with 5-OP-RU ($n = 8$) or Veh ($n = 3$ or 4), and bled for serum IL-4 and IFN-γ measurements.

(legend continued on next page)

surface CD127 levels upon exposure to glucocorticoids (Figure S6F). This phenomenon may serve as a defense mechanism at the cellular level.

In vivo studies on MAIT cells can be challenging due to the low frequency of these cells in standard mouse strains. Therefore, we used B6-MAIT^{CAST} mice that contain ~20 times more MAIT cells than do WT B6 mice (Cui et al., 2015). Subjecting these mice to prolonged restraint increased, rather than decreased, hepatic MAIT cell frequencies among αβ T cells (Figure 7C), accompanied by enhanced CD127 expression (Figure S6G). Furthermore, stress failed to reduce absolute MAIT cell numbers (Figure 7D).

To assess the impact of stress on MAIT cell functions, we first demonstrated that a single i.p. injection of 5-OP-RU gives rise to early serum IL-4 and IFN-γ spikes in B6-MAIT^{CAST} mice but not in MR1$^{-/-}$ B6-MAIT^{CAST} (MR1$^{-/-}$) MAIT-deficient animals (Figure 7E). This indicated a requirement for MAIT cells in these responses and provided us with reliable readouts to work with. B6-MAIT^{CAST} mice that had undergone restraint stress before they received 5-OP-RU had significantly lower blood levels of IL-4 and IFN-γ compared with control animals (Figure 7F). Likewise, as quickly as 30 min post-5-OP-RU administration, IL-4 and IFN-γ became detectable inside MAIT cells from control mice but not in stressed animals (Figure 7G). Therefore, stress lessens MAIT cell capacities to potentiate T_H1- and T_H2-type responses *in vivo*.

DISCUSSION

*i*T cells link the innate and adaptive arms of immunity (Matsuda et al., 2008; Rudak et al., 2018). Therefore, revealing how stress affects *i*T cell responses is important both from a basic biological standpoint and in light of their therapeutic potentials.

We demonstrate that stress compromises the ability of *i*NKT cells to trigger T_H1- and T_H2-type responses and to promote antimetastatic immune surveillance. Mechanistically, this hyporesponsive state is dependent upon direct GR signaling in *i*NKT cells, which remain uniquely and remarkably recalcitrant to glucocorticoid-inflicted apoptosis.

Many studies to date have suggested that mediators of stress promote T_H2-type immunity (Calcagni and Elenkov, 2006; Hou et al., 2013; Hu et al., 2014). Tamada et al. argued that glucocorticoids selectively retain IL-4-producing NKT cells in the T cell repertoire (Tamada et al., 1998). Our findings indicate that psychological stress limits *i*NKT cell-mediated T_H2-type responses, albeit not exclusively. In fact, stress generates a mixed inflammatory signature and also skews *i*NKT cell responses in favor of select anti-inflammatory cytokines, namely IL-10 and IL-27, but not TGF-β. To what extent these immunosuppressive cytokines inhibit T_H1 and/or T_H2 immunity following *i*NKT cell stimulation remains to be determined. We also found that stressed mice exposed to αGC generate greater levels of T_H17-associated cytokines, including IL-23 and, to a lesser degree, IL-17A. Although the exact cellular source(s) of these cytokines will need to be identified, our results point to an adaptation mechanism that may preserve fast-acting T_H17-type responses to a wide range of bacterial and fungal pathogens in the face of a stressful event.

The anticancer function of *i*NKT cells depends, in large part, on their ability to induce DC maturation and to transactivate additional effector cells (Fujii and Shimizu, 2019). These functions require the expression of CD40L and IFN-γ, both of which were reduced in *i*NKT cells during stress. Serum concentrations of multiple chemokines (e.g., IP-10, MCP-1, and RANTES) were also diminished in stressed mice receiving αGC, suggesting a weakened *i*NKT cell capacity in mobilizing other immune cell types toward inflammatory sites and infectious foci.

We found *i*NKT cells from stressed mice to launch weak cytokine responses upon *i*TCR triggering but to behave normally upon stimulation with PMA and ionomycin. Splenic *i*NKT cells from these animals had diminished *i*TCR, CD28, and ICOS levels on their surface. Further, we found reduced levels of phospho-SLP76 (pY128) and a trend toward lower phospho-CD3ζ (pY142) and phospho-ZAP70 (pY319)/phospho-Syk (pY352) levels, but not phospho-Lck (pY505), in hepatic *i*NKT cells (data not shown). These findings are consistent with a previous report that *in vitro* exposure to DEX lowers phospho-CD3ζ and phospho-ZAP70 levels, but not the kinase activity of Lck, in mouse T cells (Van Laethem et al., 2001). Deciphering the biochemical bases of the above changes and their tissue-selective patterns warrants further investigation.

The plasticity of *i*NKT cells was evident by virtue of their constitutive mRNA expression of T-bet, AP-1, nuclear factor κB (NF-κB), and nuclear factor of activated T cells (NFAT) family transcription factors (Das et al., 2010). These levels were either reduced or remained stable during stress, with the sole exception of the AP-1 subunit c-Fos. Intriguingly, the transcript levels of c-Jun, c-Fos's binding partner, were not impacted by stress. How the stoichiometric changes of Fos-Jun interactions may affect the activity of AP-1 during stress will also be a subject of future studies.

The SNS controls the activity of the HPA axis (Engeland and Arnhold, 2005), and we found *i*NKT cells to amply express adrenergic receptors. Adrenergic agonists reportedly suppress *in vivo* NK and T_{conv} cell responses (Bucsek et al., 2017; Diaz-Salazar et al., 2020; Wieduwild et al., 2020). Therefore, our finding that *i*NKT cell dysfunctions in prolonged stress stem, exclusively, from GR engagement, and not from post-ganglionic sympathetic neurotransmission, is curious. This is, however, in agreement with our recent report that OHDA-induced sympathectomy has no effect on glucocorticoid levels during prolonged stress (Rudak et al., 2019). We propose that the SNS's dominant role is likely to manifest during a fight-or-flight response to an acute stressor, which may not jeopardize *i*NKT cell functions. In fact,

(G) Stressed and control B6-MAIT^{CAST} mice were injected with 5-OP-RU (or Veh) 30 min before they were sacrificed for their liver. Hepatic MAIT cells were identified by MR1 tetramers, and IL-4$^+$ and IFN-γ$^+$ MAIT cell frequencies were determined via staining with anti-cytokine mAbs or isotype controls.

Each symbol in (A)–(D) and (G) represents an individual sample or mouse. Error bars represent SEM. *, **, ***, and **** denote differences with $p < 0.05$, $p < 0.01$, $p < 0.001$, and $p < 0.0001$, respectively, by two-way ANOVA with Dunnett's (A and B) or Tukey's (E and F) correction or by unpaired Student's t tests (C, D, and G); NS, not significant.

we have found that a brief period (15 min) of physical restraint, which results in acute stress (Dhabhar et al., 2012), fails to alter αGC-elicited cytokine production (data not shown). Consistent with the above theory, plasma NE and epinephrine levels reach their peak as early as 5–20 min after restraint in rats whereas CS levels peak later, around 60 min following physical restraint (Kvetnansky et al., 1978, 1993).

In a mouse model of cerebral stroke, Wong et al. demonstrated that NE released by post-ganglionic sympathetic neurons induces IL-10 production by hepatic *i*NKT cells, which leads to immunosuppression and secondary bacterial infection (Wong et al., 2011). However, whether or not SNS mediators, including NE, interfere with *i*TCR-mediated *i*NKT cell activation was not assessed. Nissen and coworkers reported that sustained adrenergic receptor stimulation influences the efficacy of αGC-based cancer immunotherapy only minimally (Nissen et al., 2018), and our current work indicates that SNS mediators do not appreciably impact *i*NKT cell responses to glycolipid Ags. Therefore, in the absence or presence of concomitant *i*TCR stimulation, adrenergic receptor signaling may have different outcomes.

*i*NKT cell impairments in stressed animals were accompanied by increased levels of GILZ, a transcriptional target of the GR (Monczor et al., 2019). GILZ exerts broad anti-inflammatory activities mediated, partially, by protein-protein interactions that inhibit NF-κB and AP-1 (Ronchetti et al., 2015). It has been speculated that GILZ binds directly to DNA to repress the transcription of several genes that control T cell functions (Yosef et al., 2013). GILZ was recently shown to abolish the efficacy of immunostimulatory therapies against murine tumors, and greater GILZ expression within TMEs correlated with poorer prognosis in human cancers (Yang et al., 2019). It is conceivable that GILZ contributes to suppressed *i*NKT cell functions in stressed individuals. As such, selective inhibitors of GILZ may be beneficial.

We recently reported that long-term stress upregulates the immune checkpoint molecule T cell immunoreceptor with immunoglobulin and ITIM domains (TIGIT) on *i*NKT cells in a cell-autonomous, GR-dependent fashion (Rudak et al., 2019). Our preliminary results indicate that systemic blockade of TIGIT moderately but significantly restores serum IFN-γ levels in stressed animals responding to αGC (Figure S7A). Therefore, TIGIT may be partially responsible for *i*NKT cell dysfunctions during stress, and its blockade may be a viable option in reversing stress-induced immunosuppression. Of note, *i*NKT cell responses to αGC remained impaired for at least 1 day post-stress (Figure S7B) but were restored to control levels after 1 week (Figure S7C). Therefore, although TIGIT may mediate cellular exhaustion (Johnston et al., 2014; Zhang et al., 2018), the impact of its engagement appears to be transient because *i*NKT cells from stressed mice do not exhibit signs of long-term impairments.

Consistent with the literature (Herold et al., 2006; Tseng et al., 2005), exposure to glucocorticoids contracted the size of several populations, including T_{conv}, B, and NK cells. On the contrary, however, *i*NKT and MAIT cells were resistant to glucocorticoid-induced apoptosis. Our results thus unveil a glucocorticoid-induced signaling pathway within *i*T cells that operates in a fundamentally distinctive manner. We noted that *i*NKT cells express relatively high levels of Bcl-2, which becomes even more pronounced during physical restraint. This is reminiscent of a higher Bcl-2 content in NKT cells compared with "NK1.1$^-$ T cells" as well as Bcl-2 upregulation upon radiotherapy or *in vitro* exposure to DEX as previously described (Tamada et al., 1998; Yao et al., 2009). Therefore, Bcl-2 expression may be crucial for the survival of *i*NKT cells encountering various apoptogenic stimuli, including but not limited to endogenous glucocorticoids.

GR transcriptionally controls *Cd127* in DEX-treated T cells *in vitro* (Lee et al., 2005). Here, we found GR to drive CD127 expression in *i*NKT and T_{conv} cells during stress. We also observed CD127 upregulation by hepatic mouse MAIT cells during physical confinement and also among human *i*NKT, MAIT, and T_{conv} cells exposed to HC or DEX. CD127 may allow T cells to receive survival signals counteracting the pro-apoptotic properties of endogenous glucocorticoids. Of note, we detected no changes in serum IL-7 levels immediately or shortly after restraint stress (data not shown). Nevertheless, we cannot discount a role for locally produced IL-7 in mainstream and invariant T cell homeostasis and survival in the course of a stress response. IL-7 enhances the effector functions of both *i*NKT and MAIT cells (de Lalla et al., 2008; Leeansyah et al., 2015). Therefore, its administration may be useful in bolstering *i*T cell functions in stressed subjects.

Unlike T_{conv} cells that are restricted by polymorphic MHC molecules, *i*NKT and MAIT cells recognize cognate Ags complexed with monomorphic molecules, namely CD1d and MR1, respectively (Kawano et al., 1997; Treiner et al., 2003). Therefore, CD1d and MR1 ligands should work across genetically distinct individuals, which makes *i*T cells attractive targets in immunotherapeutic interventions for microbial infections and/or malignancies (Haeryfar and Mallevaey, 2015; Rudak et al., 2018). A growing body of evidence implicates psychological stress as an obstacle to cancer immunotherapy (Levi et al., 2011; Sommershof et al., 2017; Yang et al., 2019), and our findings provide a mechanism of stress-induced immunosuppression with wide-ranging repercussions for antitumor immunity. In addition, stress curbed or drastically altered systemic inflammatory responses to αGC and 5-OP-RU, both of which are derived from microbes. It is thus likely that stress also impedes *i*T cell responses to pathogens in natural or therapeutic settings, which will be a subject of future investigations.

STAR★METHODS

Detailed methods are provided in the online version of this paper and include the following:

- KEY RESOURCES TABLE
- RESOURCE AVAILABILITY
  - Lead contact
  - Materials availability
  - Data and code availability
- EXPERIMENTAL MODEL AND SUBJECT DETAILS
  - Mice
  - Human specimens
  - Cell lines
- METHOD DETAILS

- Models of psychological stress
- Chemical sympathectomy
- Administration and pharmacological inhibition of glucocorticoids
- *In vivo* administration of *i*T cell ligands/stimuli
- Quantification of serum cytokines and CS
- Cytofluorometric analyses
- Quantitative PCR analyses
- Generation of bone marrow-derived dendritic cells (BMDCs)
- *Ex vivo* and *in vitro* treatments and stimulations
- 51-chromium (^{51}Cr) release assay
- *In vivo* killing assay
- Metastatic melanoma model

● QUANTIFICATION AND STATISTICAL ANALYSIS

SUPPLEMENTAL INFORMATION

Supplemental information can be found online at https://doi.org/10.1016/j.celrep.2021.108979.

ACKNOWLEDGMENTS

This work was funded through a Discovery Grant (04706-2019 RGPIN) from the Natural Sciences and Engineering Research Council of Canada (NSERC; to S.M.M.H.). P.T.R. is a recipient of an Alexander Graham Bell Canada Graduate Scholarship (CGS-Doctoral) from NSERC. J.C. was supported by a Careers in Immunology Fellowship from the American Association of Immunologists. V.K.K. is supported by National Institutes of Health grant R01 AI139536. O.L. is partly funded by European Research Council grant ERC-ADG-885435 and Agence Nationale de la Recherche (MAIT). Tunyalux Langsub assisted with figure preparation.

AUTHOR CONTRIBUTIONS

P.T.R. designed and performed experiments, analyzed and interpreted data, and wrote the initial manuscript. J.C. and K.M.P. performed experiments and analyzed data. K.L.S., D.N.J., and P.J.F. interpreted data. A.I.S., K.L., and V.C.M. provided clinical samples and interpreted data. V.K.K. provided experimental reagents and interpreted data. W.I. designed experiments and interpreted data. O.L. provided experimental reagents and tools, designed experiments, interpreted data, and edited the manuscript. S.M.M.H. conceived the idea, obtained funding, administered the project, designed experiments, analyzed and interpreted data, and edited the final manuscript.

DECLARATION OF INTERESTS

The authors declare no competing interests.

Received: August 3, 2020
Revised: February 9, 2021
Accepted: March 22, 2021
Published: April 13, 2021

REFERENCES

Batty, G.D., Russ, T.C., Stamatakis, E., and Kivimäki, M. (2017). Psychological distress in relation to site specific cancer mortality: pooling of unpublished data from 16 prospective cohort studies. BMJ *356*, j108.

Bereshchenko, O., Migliorati, G., Bruscoli, S., and Riccardi, C. (2019). Glucocorticoid-induced leucine zipper: a novel anti-inflammatory molecule. Front. Pharmacol. *10*, 308.

Bernin, H., Fehling, H., Marggraff, C., Tannich, E., and Lotter, H. (2016). The cytokine profile of human NKT cells and PBMCs is dependent on donor sex and stimulus. Med. Microbiol. Immunol. (Berl.) *205*, 321–332.

Blumenfeld, H.J., Tohn, R., Haeryfar, S.M., Liu, Y., Savage, P.B., and Delovitch, T.L. (2011). Structure-guided design of an invariant natural killer T cell agonist for optimum protection from type 1 diabetes in non-obese diabetic mice. Clin. Exp. Immunol. *166*, 121–133.

Bucsek, M.J., Qiao, G., MacDonald, C.R., Giridharan, T., Evans, L., Niedzwecki, B., Liu, H., Kokolus, K.M., Eng, J.W., Messmer, M.N., et al. (2017). β-adrenergic signaling in mice housed at standard temperatures suppresses an effector phenotype in CD8$^+$ T cells and undermines checkpoint inhibitor therapy. Cancer Res. *77*, 5639–5651.

Buttari, B., Profumo, E., Domenici, G., Tagliani, A., Ippoliti, F., Bonini, S., Businaro, R., Elenkov, I., and Riganò, R. (2014). Neuropeptide Y induces potent migration of human immature dendritic cells and promotes a Th2 polarization. FASEB J. *28*, 3038–3049.

Buynitsky, T., and Mostofsky, D.I. (2009). Restraint stress in biobehavioral research: recent developments. Neurosci. Biobehav. Rev. *33*, 1089–1098.

Cain, D.W., and Cidlowski, J.A. (2017). Immune regulation by glucocorticoids. Nat. Rev. Immunol. *17*, 233–247.

Calcagni, E., and Elenkov, I. (2006). Stress system activity, innate and T helper cytokines, and susceptibility to immune-related diseases. Ann. N Y Acad. Sci. *1069*, 62–76.

Cao, L., Filipov, N.M., and Lawrence, D.A. (2002). Sympathetic nervous system plays a major role in acute cold/restraint stress inhibition of host resistance to *Listeria monocytogenes*. J. Neuroimmunol. *125*, 94–102.

Chatila, T., Silverman, L., Miller, R., and Geha, R. (1989). Mechanisms of T cell activation by the calcium ionophore ionomycin. J. Immunol. *143*, 1283–1289.

Chida, Y., Hamer, M., Wardle, J., and Steptoe, A. (2008). Do stress-related psychosocial factors contribute to cancer incidence and survival? Nat. Clin. Pract. Oncol. *5*, 466–475.

Choi, J., Rudak, P.T., Lesage, S., and Haeryfar, S.M.M. (2019). Glycolipid stimulation of invariant NKT cells expands a unique tissue-resident population of precursors to mature NK cells endowed with oncolytic and antimetastatic properties. J. Immunol. *203*, 1808–1819.

Corbett, A.J., Eckle, S.B., Birkinshaw, R.W., Liu, L., Patel, O., Mahony, J., Chen, Z., Reantragoon, R., Meehan, B., Cao, H., et al. (2014). T-cell activation by transitory neo-antigens derived from distinct microbial pathways. Nature *509*, 361–365.

Crowe, N.Y., Uldrich, A.P., Kyparissoudis, K., Hammond, K.J., Hayakawa, Y., Sidobre, S., Keating, R., Kronenberg, M., Smyth, M.J., and Godfrey, D.I. (2003). Glycolipid antigen drives rapid expansion and sustained cytokine production by NK T cells. J. Immunol. *171*, 4020–4027.

Cui, Y., Franciszkiewicz, K., Mburu, Y.K., Mondot, S., Le Bourhis, L., Premel, V., Martin, E., Kachaner, A., Duban, L., Ingersoll, M.A., et al. (2015). Mucosal-associated invariant T cell-rich congenic mouse strain allows functional evaluation. J. Clin. Invest. *125*, 4171–4185.

D'Andrea, A., Goux, D., De Lalla, C., Koezuka, Y., Montagna, D., Moretta, A., Dellabona, P., Casorati, G., and Abrignani, S. (2000). Neonatal invariant Valpha24$^+$ NKT lymphocytes are activated memory cells. Eur. J. Immunol. *30*, 1544–1550.

Das, R., Sant'Angelo, D.B., and Nichols, K.E. (2010). Transcriptional control of invariant NKT cell development. Immunol. Rev. *238*, 195–215.

de Lalla, C., Festuccia, N., Albrecht, I., Chang, H.D., Andolfi, G., Benninghoff, U., Bombelli, F., Borsellino, G., Aiuti, A., Radbruch, A., et al. (2008). Innate-like effector differentiation of human invariant NKT cells driven by IL-7. J. Immunol. *180*, 4415–4424.

Dhabhar, F.S., Malarkey, W.B., Neri, E., and McEwen, B.S. (2012). Stress-induced redistribution of immune cells—from barracks to boulevards to battlefields: a tale of three hormones—Curt Richter Award winner. Psychoneuroendocrinology *37*, 1345–1368.

Diaz-Salazar, C., Bou-Puerto, R., Mujal, A.M., Lau, C.M., von Hoesslin, M., Zehn, D., and Sun, J.C. (2020). Cell-intrinsic adrenergic signaling controls the adaptive NK cell response to viral infection. J. Exp. Med. *217*, e20190549.

Dusseaux, M., Martin, E., Serriari, N., Péguillet, I., Premel, V., Louis, D., Milder, M., Le Bourhis, L., Soudais, C., Treiner, E., and Lantz, O. (2011). Human MAIT cells are xenobiotic-resistant, tissue-targeted, CD161hi IL-17-secreting T cells. Blood *117*, 1250–1259.

Elenkov, I.J., Wilder, R.L., Chrousos, G.P., and Vizi, E.S. (2000). The sympathetic nerve—an integrative interface between two supersystems: the brain and the immune system. Pharmacol. Rev. *52*, 595–638.

Engeland, W.C., and Arnhold, M.M. (2005). Neural circuitry in the regulation of adrenal corticosterone rhythmicity. Endocrine *28*, 325–332.

Flint, M.S., and Tinkle, S.S. (2001). C57BL/6 mice are resistant to acute restraint modulation of cutaneous hypersensitivity. Toxicol. Sci. *62*, 250–256.

Franciszkiewicz, K., Salou, M., Legoux, F., Zhou, Q., Cui, Y., Bessoles, S., and Lantz, O. (2016). MHC class I-related molecule, MR1, and mucosal-associated invariant T cells. Immunol. Rev. *272*, 120–138.

Franco, A.J., Chen, C., Scullen, T., Zsombok, A., Salahudeen, A.A., Di, S., Herman, J.P., and Tasker, J.G. (2016). Sensitization of the hypothalamic-pituitary-adrenal axis in a male rat chronic stress model. Endocrinology *157*, 2346–2355.

Fujii, S.I., and Shimizu, K. (2019). Immune networks and therapeutic targeting of *i*NKT cells in cancer. Trends Immunol. *40*, 984–997.

Fujii, S., Shimizu, K., Kronenberg, M., and Steinman, R.M. (2002). Prolonged IFN-gamma-producing NKT response induced with alpha-galactosylceramide-loaded DCs. Nat. Immunol. *3*, 867–874.

Fujii, S., Shimizu, K., Hemmi, H., Fukui, M., Bonito, A.J., Chen, G., Franck, R.W., Tsuji, M., and Steinman, R.M. (2006). Glycolipid alpha-C-galactosylceramide is a distinct inducer of dendritic cell function during innate and adaptive immune responses of mice. Proc. Natl. Acad. Sci. USA *103*, 11252–11257.

Girotti, M., Pace, T.W., Gaylord, R.I., Rubin, B.A., Herman, J.P., and Spencer, R.L. (2006). Habituation to repeated restraint stress is associated with lack of stress-induced c-fos expression in primary sensory processing areas of the rat brain. Neuroscience *138*, 1067–1081.

Glaser, R., and Kiecolt-Glaser, J.K. (2005). Stress-induced immune dysfunction: implications for health. Nat. Rev. Immunol. *5*, 243–251.

Gourdy, P., Araujo, L.M., Zhu, R., Garmy-Susini, B., Diem, S., Laurell, H., Leite-de-Moraes, M., Dy, M., Arnal, J.F., Bayard, F., and Herbelin, A. (2005). Relevance of sexual dimorphism to regulatory T cells: estradiol promotes IFN-gamma production by invariant natural killer T cells. Blood *105*, 2415–2420.

Haeryfar, S.M., and Berczi, I. (2001). The thymus and the acute phase response. Cell. Mol. Biol. *47*, 145–156.

Haeryfar, S.M., and Mallevaey, T. (2015). Editorial: CD1- and MR1-restricted T cells in antimicrobial immunity. Front. Immunol. *6*, 611.

Haeryfar, S.M.M., Shaler, C.R., and Rudak, P.T. (2018). Mucosa-associated invariant T cells in malignancies: a faithful friend or formidable foe? Cancer Immunol. Immunother. *67*, 1885–1896.

Hayakawa, Y., Takeda, K., Yagita, H., Kakuta, S., Iwakura, Y., Van Kaer, L., Saiki, I., and Okumura, K. (2001). Critical contribution of IFN-gamma and NK cells, but not perforin-mediated cytotoxicity, to anti-metastatic effect of alpha-galactosylceramide. Eur. J. Immunol. *31*, 1720–1727.

Herold, M.J., McPherson, K.G., and Reichardt, H.M. (2006). Glucocorticoids in T cell apoptosis and function. Cell. Mol. Life Sci. *63*, 60–72.

Hou, N., Zhang, X., Zhao, L., Zhao, X., Li, Z., Song, T., and Huang, C. (2013). A novel chronic stress-induced shift in the Th1 to Th2 response promotes colon cancer growth. Biochem. Biophys. Res. Commun. *439*, 471–476.

Hu, D., Wan, L., Chen, M., Caudle, Y., LeSage, G., Li, Q., and Yin, D. (2014). Essential role of IL-10/STAT3 in chronic stress-induced immune suppression. Brain Behav. Immun. *36*, 118–127.

Johnston, R.J., Comps-Agrar, L., Hackney, J., Yu, X., Huseni, M., Yang, Y., Park, S., Javinal, V., Chiu, H., Irving, B., et al. (2014). The immunoreceptor TIGIT regulates antitumor and antiviral CD8(+) T cell effector function. Cancer Cell *26*, 923–937.

Kamiya, A., Hayama, Y., Kato, S., Shimomura, A., Shimomura, T., Irie, K., Kaneko, R., Yanagawa, Y., Kobayashi, K., and Ochiya, T. (2019). Genetic manipulation of autonomic nerve fiber innervation and activity and its effect on breast cancer progression. Nat. Neurosci. *22*, 1289–1305.

Kawano, T., Cui, J., Koezuka, Y., Toura, I., Kaneko, Y., Motoki, K., Ueno, H., Nakagawa, R., Sato, H., Kondo, E., et al. (1997). CD1d-restricted and TCR-mediated activation of valpha14 NKT cells by glycosylceramides. Science *278*, 1626–1629.

Keller, A.N., Eckle, S.B., Xu, W., Liu, L., Hughes, V.A., Mak, J.Y., Meehan, B.S., Pediongco, T., Birkinshaw, R.W., Chen, Z., et al. (2017). Drugs and drug-like molecules can modulate the function of mucosal-associated invariant T cells. Nat. Immunol. *18*, 402–411.

Kelly, J., Minoda, Y., Meredith, T., Cameron, G., Philipp, M.S., Pellicci, D.G., Corbett, A.J., Kurts, C., Gray, D.H., Godfrey, D.I., et al. (2019). Chronically stimulated human MAIT cells are unexpectedly potent IL-13 producers. Immunol. Cell Biol. *97*, 689–699.

Kjer-Nielsen, L., Patel, O., Corbett, A.J., Le Nours, J., Meehan, B., Liu, L., Bhati, M., Chen, Z., Kostenko, L., Reantragoon, R., et al. (2012). MR1 presents microbial vitamin B metabolites to MAIT cells. Nature *491*, 717–723.

Kokolus, K.M., Capitano, M.L., Lee, C.T., Eng, J.W., Waight, J.D., Hylander, B.L., Sexton, S., Hong, C.C., Gordon, C.J., Abrams, S.I., and Repasky, E.A. (2013). Baseline tumor growth and immune control in laboratory mice are significantly influenced by subthermoneutral housing temperature. Proc. Natl. Acad. Sci. USA *110*, 20176–20181.

Kurioka, A., Jahun, A.S., Hannaway, R.F., Walker, L.J., Fergusson, J.R., Sverremark-Ekström, E., Corbett, A.J., Ussher, J.E., Willberg, C.B., and Klenerman, P. (2017). Shared and distinct phenotypes and functions of human CD161^{++} Vα7.2^{+} T cell subsets. Front. Immunol. *8*, 1031.

Kvetnansky, R., Sun, C.L., Lake, C.R., Thoa, N., Torda, T., and Kopin, I.J. (1978). Effect of handling and forced immobilization on rat plasma levels of epinephrine, norepinephrine, and dopamine-beta-hydroxylase. Endocrinology *103*, 1868–1874.

Kvetnansky, R., Fukuhara, K., Pacák, K., Cizza, G., Goldstein, D.S., and Kopin, I.J. (1993). Endogenous glucocorticoids restrain catecholamine synthesis and release at rest and during immobilization stress in rats. Endocrinology *133*, 1411–1419.

Lantz, O., and Bendelac, A. (1994). An invariant T cell receptor alpha chain is used by a unique subset of major histocompatibility complex class I-specific CD4^{+} and CD4^{-}8^{-} T cells in mice and humans. J. Exp. Med. *180*, 1097–1106.

Lee, H.C., Shibata, H., Ogawa, S., Maki, K., and Ikuta, K. (2005). Transcriptional regulation of the mouse IL-7 receptor alpha promoter by glucocorticoid receptor. J. Immunol. *174*, 7800–7806.

Leeansyah, E., Svärd, J., Dias, J., Buggert, M., Nyström, J., Quigley, M.F., Moll, M., Sönnerborg, A., Nowak, P., and Sandberg, J.K. (2015). Arming of MAIT cell cytolytic antimicrobial activity is induced by IL-7 and defective in HIV-1 infection. PLoS Pathog. *11*, e1005072.

Legoux, F., Salou, M., and Lantz, O. (2017). Unconventional or preset $\alpha\beta$ T cells: evolutionarily conserved tissue-resident T cells recognizing nonpeptidic ligands. Annu. Rev. Cell Dev. Biol. *33*, 511–535.

Lepore, M., Kalinichenko, A., Colone, A., Paleja, B., Singhal, A., Tschumi, A., Lee, B., Poidinger, M., Zolezzi, F., Quagliata, L., et al. (2014). Parallel T-cell cloning and deep sequencing of human MAIT cells reveal stable oligoclonal TCRβ repertoire. Nat. Commun. *5*, 3866.

Levi, B., Benish, M., Goldfarb, Y., Sorski, L., Melamed, R., Rosenne, E., and Ben-Eliyahu, S. (2011). Continuous stress disrupts immunostimulatory effects of IL-12. Brain Behav. Immun. *25*, 727–735.

Lisbonne, M., Hachem, P., Tonanny, M.B., Fourneau, J.M., Sidobre, S., Kronenberg, M., Van Endert, P., Dy, M., Schneider, E., and Leite-de-Moraes, M.C. (2004). *In vivo* activation of invariant V alpha 14 natural killer T cells by alpha-galactosylceramide sequentially induces Fas-dependent and -independent cytotoxicity. Eur. J. Immunol. *34*, 1381–1388.

Matsuda, J.L., Mallevaey, T., Scott-Browne, J., and Gapin, L. (2008). CD1d-restricted iNKT cells, the 'Swiss-army knife' of the immune system. Curr. Opin. Immunol. *20*, 358–368.

Mills, C.D., Kincaid, K., Alt, J.M., Heilman, M.J., and Hill, A.M. (2000). M-1/M-2 macrophages and the Th1/Th2 paradigm. J. Immunol. *164*, 6166–6173.

Monczor, F., Chatzopoulou, A., Zappia, C.D., Houtman, R., Meijer, O.C., and Fitzsimons, C.P. (2019). A model of glucocorticoid receptor interaction with coregulators predicts transcriptional regulation of target genes. Front. Pharmacol. *10*, 214.

Nakagawa, R., Inui, T., Nagafune, I., Tazunoki, Y., Motoki, K., Yamauchi, A., Hirashima, M., Habu, Y., Nakashima, H., and Seki, S. (2004). Essential role of bystander cytotoxic CD122^{+}CD8^{+} T cells for the antitumor immunity induced in the liver of mice by alpha-galactosylceramide. J. Immunol. *172*, 6550–6557.

Nissen, M.D., Sloan, E.K., and Mattarollo, S.R. (2018). β-adrenergic signaling impairs antitumor CD8^{+} T-cell responses to B-cell lymphoma immunotherapy. Cancer Immunol. Res. *6*, 98–109.

Park, S.H., Benlagha, K., Lee, D., Balish, E., and Bendelac, A. (2000). Unaltered phenotype, tissue distribution and function of Valpha14(+) NKT cells in germ-free mice. Eur. J. Immunol. *30*, 620–625.

Partecke, L.I., Speerforck, S., Käding, A., Seubert, F., Kühn, S., Lorenz, E., Schwandke, S., Sendler, M., Keßler, W., Trung, D.N., et al. (2016). Chronic stress increases experimental pancreatic cancer growth, reduces survival and can be antagonised by beta-adrenergic receptor blockade. Pancreatology *16*, 423–433.

Prod'homme, T., Weber, M.S., Steinman, L., and Zamvil, S.S. (2006). A neuropeptide in immune-mediated inflammation, Y? Trends Immunol. *27*, 164–167.

Pruett, S.B. (2003). Stress and the immune system. Pathophysiology *9*, 133–153.

Rahimpour, A., Koay, H.F., Enders, A., Clanchy, R., Eckle, S.B., Meehan, B., Chen, Z., Whittle, B., Liu, L., Fairlie, D.P., et al. (2015). Identification of phenotypically and functionally heterogeneous mouse mucosal-associated invariant T cells using MR1 tetramers. J. Exp. Med. *212*, 1095–1108.

Ronchetti, S., Migliorati, G., and Riccardi, C. (2015). GILZ as a mediator of the anti-inflammatory effects of glucocorticoids. Front. Endocrinol. (Lausanne) *6*, 170.

Rudak, P.T., Choi, J., and Haeryfar, S.M.M. (2018). MAIT cell-mediated cytotoxicity: roles in host defense and therapeutic potentials in infectious diseases and cancer. J. Leukoc. Biol. *104*, 473–486.

Rudak, P.T., Gangireddy, R., Choi, J., Burhan, A.M., Summers, K.L., Jackson, D.N., Inoue, W., and Haeryfar, S.M.M. (2019). Stress-elicited glucocorticoid receptor signaling upregulates TIGIT in innate-like invariant T lymphocytes. Brain Behav. Immun. *80*, 793–804.

Salio, M., Gasser, O., Gonzalez-Lopez, C., Martens, A., Veerapen, N., Gileadi, U., Verter, J.G., Napolitani, G., Anderson, R., Painter, G., et al. (2017). Activation of human mucosal-associated invariant T cells induces CD40L-dependent maturation of monocyte-derived and primary dendritic cells. J. Immunol. *199*, 2631–2638.

Salou, M., Legoux, F., Gilet, J., Darbois, A., du Halgouet, A., Alonso, R., Richer, W., Goubet, A.G., Daviaud, C., Menger, L., et al. (2019). A common transcriptomic program acquired in the thymus defines tissue residency of MAIT and NKT subsets. J. Exp. Med. *216*, 133–151.

Saul, A.N., Oberyszyn, T.M., Daugherty, C., Kusewitt, D., Jones, S., Jewell, S., Malarkey, W.B., Lehman, A., Lemeshow, S., and Dhabhar, F.S. (2005). Chronic stress and susceptibility to skin cancer. J. Natl. Cancer Inst. *97*, 1760–1767.

Schmieg, J., Yang, G., Franck, R.W., and Tsuji, M. (2003). Superior protection against malaria and melanoma metastases by a C-glycoside analogue of the natural killer T cell ligand alpha-galactosylceramide. J. Exp. Med. *198*, 1631–1641.

Schober, A. (2004). Classic toxin-induced animal models of Parkinson's disease: 6-OHDA and MPTP. Cell Tissue Res. *318*, 215–224.

Smyth, M.J., Crowe, N.Y., Pellicci, D.G., Kyparissoudis, K., Kelly, J.M., Takeda, K., Yagita, H., and Godfrey, D.I. (2002). Sequential production of interferon-gamma by NK1.1(+) T cells and natural killer cells is essential for the antimetastatic effect of alpha-galactosylceramide. Blood *99*, 1259–1266.

Sommershof, A., Scheuermann, L., Koerner, J., and Groettrup, M. (2017). Chronic stress suppresses anti-tumor T_{CD8+} responses and tumor regression following cancer immunotherapy in a mouse model of melanoma. Brain Behav. Immun. *65*, 140–149.

Straub, R.H., Schaller, T., Miller, L.E., von Hörsten, S., Jessop, D.S., Falk, W., and Schölmerich, J. (2000). Neuropeptide Y cotransmission with norepinephrine in the sympathetic nerve-macrophage interplay. J. Neurochem. *75*, 2464–2471.

Tamada, K., Harada, M., Abe, K., Li, T., and Nomoto, K. (1998). IL-4-producing NK1.1^{+} T cells are resistant to glucocorticoid-induced apoptosis: implications for the Th1/Th2 balance. J. Immunol. *161*, 1239–1247.

Tang, X.Z., Jo, J., Tan, A.T., Sandalova, E., Chia, A., Tan, K.C., Lee, K.H., Gehring, A.J., De Libero, G., and Bertoletti, A. (2013). IL-7 licenses activation of human liver intrasinusoidal mucosal-associated invariant T cells. J. Immunol. *190*, 3142–3152.

Taves, M.D., and Ashwell, J.D. (2020). Glucocorticoids in T cell development, differentiation and function. Nat. Rev. Immunol. Published online November 4, 2020. https://doi.org/10.1038/s41577-020-00464-0.

Treiner, E., Duban, L., Bahram, S., Radosavljevic, M., Wanner, V., Tilloy, F., Affaticati, P., Gilfillan, S., and Lantz, O. (2003). Selection of evolutionarily conserved mucosal-associated invariant T cells by MR1. Nature *422*, 164–169.

Tseng, R.J., Padgett, D.A., Dhabhar, F.S., Engler, H., and Sheridan, J.F. (2005). Stress-induced modulation of NK activity during influenza viral infection: role of glucocorticoids and opioids. Brain Behav. Immun. *19*, 153–164.

Tyznik, A.J., Tupin, E., Nagarajan, N.A., Her, M.J., Benedict, C.A., and Kronenberg, M. (2008). Cutting edge: the mechanism of invariant NKT cell responses to viral danger signals. J. Immunol. *181*, 4452–4456.

van den Heuvel, M.J., Garg, N., Van Kaer, L., and Haeryfar, S.M. (2011). NKT cell costimulation: experimental progress and therapeutic promise. Trends Mol. Med. *17*, 65–77.

Van Laethem, F., Baus, E., Smyth, L.A., Andris, F., Bex, F., Urbain, J., Kioussis, D., and Leo, O. (2001). Glucocorticoids attenuate T cell receptor signaling. J. Exp. Med. *193*, 803–814.

van Wilgenburg, B., Scherwitzl, I., Hutchinson, E.C., Leng, T., Kurioka, A., Kulicke, C., de Lara, C., Cole, S., Vasanawathana, S., Limpitikul, W., et al.; STOP-HCV Consortium (2016). MAIT cells are activated during human viral infections. Nat. Commun. *7*, 11653.

Velázquez, P., Cameron, T.O., Kinjo, Y., Nagarajan, N., Kronenberg, M., and Dustin, M.L. (2008). Cutting edge: activation by innate cytokines or microbial antigens can cause arrest of natural killer T cell patrolling of liver sinusoids. J. Immunol. *180*, 2024–2028.

Watanabe, H., Numata, K., Ito, T., Takagi, K., and Matsukawa, A. (2004). Innate immune response in Th1- and Th2-dominant mouse strains. Shock *22*, 460–466.

Wieduwild, E., Girard-Madoux, M.J., Quatrini, L., Laprie, C., Chasson, L., Rossignol, R., Bernat, C., Guia, S., and Ugolini, S. (2020). β2-adrenergic signals downregulate the innate immune response and reduce host resistance to viral infection. J. Exp. Med. *217*, e20190554.

Wong, C.H., Jenne, C.N., Lee, W.Y., Léger, C., and Kubes, P. (2011). Functional innervation of hepatic *i*NKT cells is immunosuppressive following stroke. Science *334*, 101–105.

Yang, H., Xia, L., Chen, J., Zhang, S., Martin, V., Li, Q., Lin, S., Chen, J., Calmette, J., Lu, M., et al. (2019). Stress-glucocorticoid-TSC22D3 axis compromises therapy-induced antitumor immunity. Nat. Med. *25*, 1428–1441.

Yao, Z., Liu, Y., Jones, J., and Strober, S. (2009). Differences in Bcl-2 expression by T-cell subsets alter their balance after *in vivo* irradiation to favor CD4^{+}Bcl-2hi NKT cells. Eur. J. Immunol. *39*, 763–775.

Yao, T., Shooshtari, P., and Haeryfar, S.M.M. (2020). Leveraging public single-cell and bulk transcriptomic datasets to delineate MAIT cell roles and phenotypic characteristics in human malignancies. Front. Immunol. *11*, 1691.

Yin, D., Tuthill, D., Mufson, R.A., and Shi, Y. (2000). Chronic restraint stress promotes lymphocyte apoptosis by modulating CD95 expression. J. Exp. Med. *191*, 1423–1428.

Yosef, N., Shalek, A.K., Gaublomme, J.T., Jin, H., Lee, Y., Awasthi, A., Wu, C., Karwacz, K., Xiao, S., Jorgolli, M., et al. (2013). Dynamic regulatory network controlling TH17 cell differentiation. Nature *496*, 461–468.

Zhang, Q., Bi, J., Zheng, X., Chen, Y., Wang, H., Wu, W., Wang, Z., Wu, Q., Peng, H., Wei, H., et al. (2018). Blockade of the checkpoint receptor TIGIT prevents NK cell exhaustion and elicits potent anti-tumor immunity. Nat. Immunol. *19*, 723–732.

Zhang, Y., Springfield, R., Chen, S., Li, X., Feng, X., Moshirian, R., Yang, R., and Yuan, W. (2019). α-GalCer and *i*NKT cell-based cancer immunotherapy: realizing the therapeutic potentials. Front. Immunol. *10*, 1126.

STAR★METHODS

KEY RESOURCES TABLE

REAGENT or RESOURCE	SOURCE	IDENTIFIER
Antibodies		
Alexa 700-conjugated anti-mouse/human B220 (Clone RA3-6B2)	Thermo Fisher Scientific	Cat # 56-0452-82; RRID: AB_891458
Alexa 700-conjugated anti-human CD3 (Clone UCHT1)	Thermo Fisher Scientific	Cat # 56-0038-42; RRID: AB_10597906
PE-Cy7-conjugated anti-mouse CD3ε (Clone 145-2C11)	Thermo Fisher Scientific	Cat # 25-0031-82; RRID: AB_469572
FITC-conjugated anti-mouse CD4 (Clone GK1.5)	Thermo Fisher Scientific	Cat # 11-0041-81; RRID: AB_464891
PE-eFluor610-conjugated anti-mouse CD11c (Clone N418)	Thermo Fisher Scientific	Cat # 61-0114-80; RRID: AB_2574529
PE-conjugated anti-mouse CD25 (Clone PC61.5)	Thermo Fisher Scientific	Cat # 12-0251-81; RRID: AB_465606
PerCP-Cy5.5-conjugated anti-mouse CD28 (Clone 37.51)	Thermo Fisher Scientific	Cat # 45-0281-80; RRID: AB_925744
PE-Cy5-conjugated anti-mouse/human CD44 (Clone IM7)	Thermo Fisher Scientific	Cat # 15-0441-81; RRID: AB_468748
FITC-conjugated anti-mouse/human CD44 (Clone IM7)	Thermo Fisher Scientific	Cat # 11-0441-81; RRID: AB_465044
PE-conjugated anti-mouse CD45 (Clone 30-F11)	Thermo Fisher Scientific	Cat # 12-0451-82; RRID: AB_465668
APC-eFluor780-conjugated anti-mouse CD62L (Clone MEL-14)	Thermo Fisher Scientific	Cat # 47-0621-80; RRID: AB_1603258
PerCP-Cy5.5-conjugated anti-mouse CD69 (Clone H1.2F3)	Thermo Fisher Scientific	Cat # 45-0691-82; RRID: AB_1210703
PE-conjugated anti-mouse CD127 (Clone A7R34)	Thermo Fisher Scientific	Cat # 12-1271-82; RRID: AB_465844
PerCP-Cy5.5-conjugated anti-human CD127 (Clone eBioRDR5)	Thermo Fisher Scientific	Cat # 45-1278-41; RRID: AB_10669708
FITC-conjugated anti-mouse/rat/Rhesus monkey CD278/ICOS (Clone C398.4A)	Thermo Fisher Scientific	Cat # 11-9949-82; RRID: AB_465458
PE-Cy7-conjugated anti-mouse NK1.1 (Clone PK136)	Thermo Fisher Scientific	Cat # 25-5941-82; RRID: AB_469665
FITC-conjugated anti-mouse TCRβ (Clone H57-597)	Thermo Fisher Scientific	Cat # 11-5961-85; RRID: AB_465324
PE-Cy7-conjugated anti-mouse TCRβ (Clone H57-597)	Thermo Fisher Scientific	Cat # 25-5961-82; RRID: AB_2573507
APC-eFluor780-conjugated anti-mouse TCRβ (Clone H57-597)	Thermo Fisher Scientific	Cat # 47-5961-82; RRID: AB_1272173
PE-Cy7-conjugated anti-mouse/rat Bcl-2 (Clone 10C4)	Thermo Fisher Scientific	Cat # 25-6992-42; RRID: AB_2573516
PE-conjugated anti-mouse/human GILZ (Clone CFMKG15)	Thermo Fisher Scientific	Cat # 12-4033-80; RRID: AB_1659717
PE-conjugated anti-mouse IFN-γ (Clone XMG1.2)	Thermo Fisher Scientific	Cat # 12-7311-82; RRID: AB_466193
PE-Cy7-conjugated anti-mouse IL-2 (Clone JES6-5H4)	Thermo Fisher Scientific	Cat # 25-7021-82; RRID: AB_1235004
PE-Cy7-conjugated anti-mouse IL-4 (Clone 11B11)	BD Biosciences	Cat # 560699; RRID: AB_1727548
PE-Cy7-conjugated anti-mouse IL-4 (Clone BVD6-24G2)	Thermo Fisher Scientific	Cat # 25-7042-82; RRID: AB_469674
PE-conjugated anti-mouse/human IL-5 (Clone TRFK5)	Thermo Fisher Scientific	Cat # 12-7052-81; RRID: AB_763588
eFluor660-conjugated anti-mouse IL-12p35 (Clone 4D10p35)	Thermo Fisher Scientific	Cat # 50-7352-80; RRID: AB_2574284
APC-eFluor780-conjugated anti-mouse IL-13 (Clone eBio13A)	Thermo Fisher Scientific	Cat # 47-7133-80; RRID: AB_2716963
PerCP-eFluor710-conjugated anti-mouse/rat/human/ non-human primate/cynomolgus monkey/dog Ki67 (Clone SolA15)	Thermo Fisher Scientific	Cat # 46-5698-82; RRID: AB_11040981
PE-conjugated anti-mouse/rat/human/guinea pig/rabbit/ sheep/yeast glucocorticoid receptor (Clone BuGR2)	Novus Biologicals	Cat # NB300-731PE; RRID: AB_2298869
PE-Cy5-conjugated rat IgG2bκ isotype control (Clone eB149/10H5)	Thermo Fisher Scientific	Cat # 15-4031-82; RRID: AB_470133
FITC-conjugated rat IgG2bκ isotype control (Clone Eb149/10H5)	Thermo Fisher Scientific	Cat # 11-4031-81; RRID: AB_470003
APC-eFluor780-conjugated rat IgG2aκ isotype control (Clone eBR2a)	Thermo Fisher Scientific	Cat # 47-4321-80; RRID: AB_1272001
PerCP-Cy5.5-conjugated Armenian hamster IgG isotype control (Clone eBio299Arm)	Thermo Fisher Scientific	Cat # 45-4888-80; RRID: AB_906260
PE-conjugated rat IgG2aκ isotype control (Clone eBR2a)	Thermo Fisher Scientific	Cat # 12-4321-42; RRID: AB_1518773
PerCP-Cy5.5-conjugated mouse IgG1κ isotype control (Clone P3.6.2.8.1)	Thermo Fisher Scientific	Cat # 45-4714-82; RRID: AB_906257
PE-Cy7-conjugated mouse IgG1κ isotype control (Clone P3.6.2.8.1)	Thermo Fisher Scientific	Cat # 25-4714-42; RRID: AB_1548705
PE-conjugated rat IgG1κ isotype control (Clone eBRG1)	Thermo Fisher Scientific	Cat # 12-4301-82; RRID: AB_470047

(*Continued on next page*)

Continued

REAGENT or RESOURCE	SOURCE	IDENTIFIER
PE-Cy7-conjugated rat IgG2bκ isotype control (Clone eB149/10H5)	Thermo Fisher Scientific	Cat # 25-4031-82; RRID: AB_891624
eFluor660-conjugated rat IgG2aκ isotype control (Clone eBR2a)	Thermo Fisher Scientific	Cat # 50-4321-80; RRID: AB_10598640
APC-eFluor780-conjugated rat IgG1κ isotype control (Clone eBRG1)	Thermo Fisher Scientific	Cat # 47-4301-80; RRID: AB_1271986
PE-Cy7-conjugated rat IgG1κ isotype control (Clone R3-34)	BD Biosciences	Cat # 557645; RRID: AB_396762
PE-Cy7-conjugated rat IgG1κ isotype control (Clone eBRG1)	Thermo Fisher Scientific	Cat # 25-4301-82; RRID: AB_470198
PerCP-eFluor 710-conjugated rat IgG2aκ isotype control (Clone eBR2a)	Thermo Fisher Scientific	Cat # 46-4321-82; RRID: AB_1834455
PE-conjugated mouse IgG2aκ isotype control (Clone G155-178)	BD Biosciences	Cat # 556653; RRID: AB_396517
PE-Cy7-conjugated Armenian hamster IgG isotype control (Clone eBio299Arm)	Thermo Fisher Scientific	Cat # 25-4888-82; RRID: AB_470204
FITC-conjugated Armenian hamster IgG isotype control (Clone eBio299Arm)	Thermo Fisher Scientific	Cat # 11-4888-85; RRID: AB_470038
PE-conjugated rat IgG2bκ isotype control (Clone eB149/10H5)	Thermo Fisher Scientific	Cat # 12-4031-82; RRID: AB_470042
Anti-mouse/rat tyrosine hydroxylase (polyclonal)	Abcam	Cat # ab117112
Anti-mouse/rat/human/cow/fruit fly/sheep/plant/ *Xenopus*/yeast/zebrafish β-actin (Clone mAbGEa)	Thermo Fisher Scientific	Cat # MA1-744; RRID: AB_2223496
HRP-conjugated goat anti-Rabbit IgG (H+L) (Polyclonal)	Thermo Fisher Scientific	Cat # 31460; RRID: AB_228341
HRP-conjugated goat anti-mouse IgG (H+L) (Polyclonal)	Thermo Fisher Scientific	Cat # 31430; RRID: AB_228307
Anti-mouse TIGIT (Clone 1B4)	Cell Essentials, Inc. (Boston, MA): http://www.cell-essentials.com	Lot # 111704
Mouse IgG1κ isotype control (Clone MOPC-21)	BioXCell	Cat # BE0083; RRID: AB_1107784
Biological samples		
Human tumor-free liver samples	This paper/University Hospital at London Health Sciences Centre	N/A
Healthy human blood samples	This paper	N/A
Chemicals, peptides, and recombinant proteins		
APC- or PE-conjugated PBS-57-loaded mouse or human CD1d tetramer	NIH Tetramer Core Facility	N/A
APC- or PE-conjugated unloaded mouse or human CD1d tetramer	NIH Tetramer Core Facility	N/A
APC- or PE-conjugated 5-OP-RU-loaded mouse or human MR1 tetramer (Corbett et al., 2014)	NIH Tetramer Core Facility	N/A
APC- or PE-conjugated 6-FP-loaded mouse or human MR1 tetramer (Corbett et al., 2014)	NIH Tetramer Core Facility	N/A
αGC	Funakoshi	Cat # KRN7000
αCGC	NIH Tetramer Core Facility	N/A
5-amino-6-D-ribitylaminouracil (5-ARU)	Dr. Olivier Lantz	N/A
Methylglyoxal solution	Sigma-Aldrich	Cat # M0252
Phorbol 12-myristate 13-acetate (PMA)	Sigma-Aldrich	Cat # P1585
Ionomycin	Sigma-Aldrich	Cat # I9657
Brefeldin A	Sigma-Aldrich	Cat # B7651
Recombinant mouse GM-CSF	Peprotech	Cat # 315-03
Recombinant mouse IL-4	Peprotech	Cat # 214-14
Recombinant mouse IL-12p70	Peprotech	Cat # 210-12
Recombinant mouse IL-18	R&D Systems	Cat # 9139-IL-050
6-hydroxydopamine hydrobromide	Sigma-Aldrich	Cat # 162957
Corticosterone	Sigma-Aldrich	Cat # 27840

(*Continued on next page*)

Continued

REAGENT or RESOURCE	SOURCE	IDENTIFIER
Hydrocortisone	Sigma-Aldrich	Cat # H0888
Dexamethasone	Sigma-Aldrich	Cat # D4902
Metyrapone	Sigma-Aldrich	Cat # M2696
RU486	Sigma-Aldrich	Cat # M8046
Norepinephrine	Sigma-Aldrich	Cat # A7257
Neuropeptide Y	Sigma-Aldrich	Cat # N5017
Propranolol hydrochloride	Sigma-Aldrich	Cat # P0884
Percoll PLUS	GE Healthcare	Cat # 17-5445-01
Ficoll-Paque PLUS	GE Healthcare	Cat # 17-1440-02
$Na_2{}^{51}CrO_4$	PerkinElmer	Cat # NEZ030S001MC
Triton X-100	Sigma-Aldrich	Cat # T8787
XenoLight D-Luciferin	PerkinElmer	Cat # 127799
7-aminoactinomycin D (7-AAD) viability dye	Thermo Fisher Scientific	Cat # 00-6993-50
Critical commercial assays		
Amersham ECL Prime Western Blotting Detection Reagent	GE Healthcare	Cat # RPN2232
eBioscience Ready-SET-Go! Mouse IFN-γ ELISA Kit	Thermo Fisher Scientific	Cat # 88-7314-88
eBioscience Ready-SET-Go! Mouse IL-2 ELISA Kit	Thermo Fisher Scientific	Cat # 88-7024-88
eBioscience Ready-SET-Go! Mouse IL-4 ELISA Kit	Thermo Fisher Scientific	Cat # 88-7044-88
DetectX Corticosterone Enzyme Immunoassay Kit	Arbor Assays	Cat # K014-H1
Intracellular Fixation & Permeabilization Buffer Set	Thermo Fisher Scientific	Cat # 88-8824-00
Foxp3/Transcription Factor Staining Buffer Set	Thermo Fisher Scientific	Cat # 00-5523-00
FITC CaspaTag Pan-Caspase *In Situ* Assay Kit	EMD Millipore	Cat # APT420
EasySep Mouse CD11c Positive Selection Kit II	STEMCELL Technologies	Cat # 18780A
PureLink RNA Mini Kit	Thermo Fisher Scientific	Cat # 12183018A
SuperScript VILO cDNA Synthesis Kit	Thermo Fisher Scientific	Cat # 11755-050
Taqman Fast Advanced Master Mix	Thermo Fisher Scientific	Cat # 4444557
CellTrace CFSE Cell Proliferation Kit	Thermo Fisher Scientific	Cat # C34554
Experimental models: Cell lines		
Mouse: YAC-1 lymphoma cells	ATCC	Cat # TIB-160; RRID: CVCL_2244
Mouse: B16-F10 melanoma cells	Dr. Ann Chambers, Western University	Available from ATCC (Cat # CRL-6475; RRID: CVCL_0159)
Mouse: B16-F10-Red-FLuc (B16-FLuc) melanoma cells	PerkinElmer	Cat # BW124734
Mouse: DN32.D3 hybridoma cells	Dr. Albert Bendelac, University of Chicago	N/A
Experimental models: Organisms/strains		
Mouse: C57BL/6	Charles River Canada	Cat # 027; RRID: IMSR_CRL:027
Mouse: BALB/c	Charles River Canada	Cat # 028; RRID: IMSR_CRL:028
Mouse: β2M$^{-/-}$: B6.129P2-B2m^{tm1Unc}/DcrJ	Dr. Anthony Jevnikar, Western University	Available from The Jackson Laboratory (Cat # 002087; RRID: IMSR_JAX:002087)
Mouse: B6 albino: B6(Cg)-Tyr^{c-2J}/J	The Jackson Laboratory	Cat # 000058; RRID: IMSR_JAX:000058
Mouse: B6.Nr3c1$^{fl/fl}$: B6.Cg-Nr3c1$^{tm1.1Jda}$/J	The Jackson Laboratory	Cat # 021021; RRID: IMSR_JAX:021021
Mouse: B6.Lck$^{cre/cre}$: B6.Cg-Tg(Lck-cre)548Jxm/J	The Jackson Laboratory	Cat # 003802; RRID: IMSR_JAX:003802
Mouse: Nr3c1^{fl}Lck^{cre}: B6.Nr3c1$^{fl/fl}$Lck$^{cre/wt}$	This paper	N/A
Mouse: Lck^{cre}: B6.Lck$^{cre/wt}$	This paper	N/A
Mouse: B6-MAIT^{CAST} (Cui et al., 2015)	Dr. Olivier Lantz	N/A
Mouse: MR1$^{-/-}$ B6-MAIT^{CAST} (Cui et al., 2015)	Dr. Olivier Lantz	N/A

(*Continued on next page*)

Continued

REAGENT or RESOURCE	SOURCE	IDENTIFIER
Oligonucleotides		
See Table S1 for qPCR primer/probe sets	Thermo Fisher Scientific	N/A
Software and algorithms		
FlowJo version 10.0.7 software	Tree Star	https://www.flowjo.com/
Image Studio version 3.1.4 software	LI-COR Biosciences	https://www.licor.com/bio/image-studio/
LivingImage software	PerkinElmer	https://www.perkinelmer.com/product/spectrum-200-living-image-v4series-1-128113
GraphPad Prism version 6.0 software	GraphPad	https://www.graphpad.com/

RESOURCE AVAILABILITY

Lead contact

Further information and requests for resources and reagents should be directed to and will be fulfilled by the Lead Contact, Dr. Mansour Haeryfar (Mansour.Haeryfar@schulich.uwo.ca).

Materials availability

The B6.Nr3c1$^{fl/fl}$Lck$^{cre/wt}$ and B6.Lck$^{cre/wt}$ mouse lines generated in this study can be bred using commercially available parental strains as described under Experimental model and subject details. This study did not generate any other new unique reagents.

Data and code availability

This study did not generate/analyze datasets or codes.

EXPERIMENTAL MODEL AND SUBJECT DETAILS

Mice

Adult WT B6 and BALB/c mice, between 8 and 16 weeks of age, were purchased from Charles River Canada (Saint-Constant, QC). B6(Cg)-Tyr^{c-2J}/J (B6 albino) mice (#000058) were purchased from The Jackson Laboratory (Bar Harbor, ME). B6-MAIT^{CAST} mice, a congenic strain harboring a larger MAIT cell compartment relative to WT B6 mice, and MAIT cell-deficient MR1$^{-/-}$ B6-MAIT^{CAST} mice have been previously described (Cui et al., 2015). β2M$^{-/-}$ mice were provided by Dr. Anthony Jevnikar (Western University, London, ON). Nr3c1^{fl}Lck^{cre} mice, whose T cells lack the GR, were generated by crossing B6.Nr3c1$^{fl/fl}$ (Jackson #021021) with B6.Lck$^{cre/cre}$ mice (Jackson #003802), followed by backcrossing the offspring with Nr3c1^{fl} mice. Lck^{cre} mice were generated by crossing offspring with WT B6 mice. PCR-based genotyping was conducted throughout breeding. Animals were housed in an institutional barrier facility with constant light/dark cycles. Prior to any experiment, mice were randomly assigned to treatment groups. Both male and female mice were included in our initial serum cytokine analyses (Figures 1B, 1C, 7E, 7F, and S2) and immunophenotyping studies (Figures 2A, 2B, 7C, and 7D). Male mice were used in all other *in vivo* experiments. Cohorts were always age- and sex-matched. Mouse experiments were conducted following Animal Use Protocols 2010-241, 2018-093 and 2018-130, which were approved by the Animal Care Committee of Animal Care and Veterinary Services at Western University.

Human specimens

HMNCs were obtained from tumor-free liver samples from patients undergoing surgical resection, without prior neoadjuvant therapy, at University Hospital (London Health Sciences Centre, London, ON). Three patients had undergone surgery for colorectal liver metastasis, one for ampullary cancer, one for ampullary adenoma, and one for pancreatic cancer. Patients had a mean age of 64 (range: 37-80) and were all male.

PBMCs were isolated from 4 healthy blood donors, two males and two females, with a mean age of 37 (range: 29-51). Human specimens were collected after obtaining written, informed consent from participants as per study protocols 5545, 2597 and 113362 approved by the Western University Research Ethics Board for Health Sciences Research Involving Human Subjects.

Cell lines

The mouse lymphoma cell line YAC-1 (ATCC TIB-160) was grown at 37°C in RPMI 1640 medium supplemented with 10% fetal bovine serum (FBS), 2 mM GlutaMAX-I, 0.1 mM MEM nonessential amino acids, 1mM sodium pyruvate, 100 U/mL penicillin, 100 μg/mL

streptomycin, and 10 mM HEPES, which has been referred to as complete medium. The mouse melanoma line B16-F10 was provided by Dr. Ann Chambers (Western University, London, ON) and maintained in MEM Alpha medium supplemented with 10% FBS. Luciferase-expressing B16-FLuc cells (PerkinElmer #BW124734) were grown in RPMI 1640 containing 10% FBS. DN32.D3, a $CD4^{-}CD8^{-}$ *i*NKT hybridoma cell line from Dr. Albert Bendelac (University of Chicago, Chicago, IL), was cultured in RPMI 1640 containing 10% FBS, 2 mM GlutaMAX-I, and 0.1 mM MEM nonessential amino acids.

METHOD DETAILS

Models of psychological stress

To induce prolonged confinement stress, mice were held horizontally for 12 h inside well-ventilated 50-mL conical tubes. This immobilization procedure prompts psychological stress in rodents without causing pain or physical compression and activates the SNS and the HPA axis (Buynitsky and Mostofsky, 2009). Cage-mate controls remained undisturbed but were deprived of access to food and water for 12 h. To model acute stress, mice were restrained for 15 minutes (Dhabhar et al., 2012) while control animals were left in home cages without food and water.

Repeated restraint stress (RRS) was inflicted by subjecting mice to 21 days of physical immobilization for 1 h daily. The experimenter and the time at which each stressor was applied remained constant throughout the entire procedure.

The chronic variable stress (CVS) model entailed daily exposures to heterotypic psychological or physical stressors for 21 days. One brief stressor during the light cycle and one overnight (O/N) stressor during the dark cycle were introduced each day. In no particular order, brief stressors included placement in a 4°C environment for 1 h, physical restraint for 1 h, horizontal cage shaking at 80 rpm for 1 h, and placement in 30°C water for 15 minutes. O/N stressors included water deprivation, cage tilting at a 45-degree angle, constant exposure to light, wet bedding (through pouring ~200 mL of water onto cage bedding), and food deprivation. Unlike RRS, mice fail to habituate to unpredictable stressors in the CVS model and display continuously elevated stress responses as a consequence (Franco et al., 2016). Parallel cohorts of non-stressed control mice were left undisturbed with food and water *ad libitum* for 21 days.

Chemical sympathectomy

Six days before mice were subjected to prolonged restraint stress, 6-hydroxydopamine (OHDA) (Sigma-Aldrich) was administered i.p. at 200 mg/kg in a vehicle containing 0.9% NaCl and 10^{-7} M ascorbic acid in phosphate-buffered saline (PBS). Successful sympathectomy was confirmed by immunoblotting for TH in splenic and brain tissues of OHDA-treated mice. We used a rabbit polyclonal Ab (ab117112 from abcam) to capture mouse TH, and an anti-mouse β-actin mAb (mAbGEa from Thermo Scientific) served as a loading control. Horseradish peroxidase-conjugated goat anti-rabbit IgG and anti-mouse IgG secondary Abs were from Thermo Scientific. Enzymatic reactions were initiated using the Amersham ECL Prime Western Blotting Detection Reagent (GE Healthcare). Blots were digitally imaged using a C-DiGit Blot Scanner (LI-COR Biosciences).

Administration and pharmacological inhibition of glucocorticoids

To simulate stress-elicited rise in glucocorticoids, corticosterone (CS) (Sigma-Aldrich) was administered orally. CS was dissolved in absolute ethanol and then diluted in standard drinking water to yield a final concentration of 25 μg/mL of water with 1% ethanol. CS-containing water was provided for 21 days with weekly replenishments. This regimen gives rise to CS serum levels that are comparable to those found in chronically stressed mice as we previously reported (Rudak et al., 2019).

In several experiments, mice were injected i.p. with 200 mg/kg of the glucocorticoid synthesis inhibitor metyrapone (Sigma-Aldrich) or with 25 mg/kg of the GR antagonist RU486 (Sigma-Aldrich) 1 h prior to prolonged restraint stress.

In vivo administration of *i*T cell ligands/stimuli

Glycolipid stimulation of *i*NKT cells was achieved via i.p. administration of 100 μg/kg of KRN7000/αGC (Funakoshi, Tokyo, Japan) or 200 μg/kg of αCGC in a vehicle containing 5.6% sucrose, 0.75% L-histidine and 0.5% Tween-20, which was further diluted in PBS. αCGC was supplied by the NIH Tetramer Core Facility (Atlanta, GA). To stimulate *i*NKT cells in a cytokine-dependent manner, each animal was injected i.v. with 2 ng recombinant mouse IL-12 (Peprotech, Rocky Hill, NJ) plus 200 ng recombinant mouse IL-18 (R&D Systems) in PBS.

To activate MAIT cells, mice were injected i.p. with 200 μL of PBS containing 20 μL of a 5-OP-RU stock solution. The stock solution was prepared by mixing equal volumes of 2 mM 5-amino-6-D-ribitylaminouracil (5-ARU) and 2 mM methylglyoxal in DMSO for 24 h at room temperature. Aliquots were stored at −80°C until use. Control mice received vehicle (2 mM methylglyoxal in DMSO) diluted in PBS.

Where indicated, mice were given 200 μg of a TIGIT-blocking mAb (clone 1B4) or a mouse IgG1κ isotype control (clone MOPC-21 from BioXCell) 1 h prior to αGC administration.

Quantification of serum cytokines and CS

Mice were bled immediately after stress or at 2, 12 and 24 h post-treatment with αGC, αCGC, 5-OP-RU, or an appropriate vehicle. Sera were isolated, aliquoted and stored at −20°C. Mouse IFN-γ, IL-2 and IL-4 concentrations were measured using eBioscience

Ready-SET-Go! ELISA Kits. Cytokine multiplex analyses were performed by Eve Technologies (Calgary, AB). CS levels were measured using a DetectX Corticosterone Enzyme Immunoassay kit (Arbor Assays, Ann Arbor, MI).

Cytofluorometric analyses

After cervical dislocation, mouse spleens were mechanically homogenized and depleted of erythrocytes through exposure to ACK (Ammonium-Chlorine-Potassium) lysis buffer for 3 minutes at room temperature. HMNCs were isolated from mouse livers or human tumor-free liver samples. Specimens were homogenized, and parenchymal cells were removed by density gradient centrifugation at 700 × *g* in 33.75% Percoll PLUS (GE Healthcare). This was followed by treatment with ACK lysis buffer to eliminate erythrocytes. To isolate human PBMCs, uncoagulated blood from healthy donors was spun at 1,200 × *g* in 50 mL SepMate PBMC Isolation Tubes (STEMCELL Technologies) containing Ficoll-Paque PLUS (GE Healthcare).

Before surface staining, mouse cell suspensions were incubated for 10 minutes on ice with 5 μg/mL of an anti-mouse CD16/CD32 mAb (clone 2.4G2) to prevent non-specific binding to Fcγ receptors. Cell surface staining was conducted for 30 minutes at 4°C in PBS containing 2% FBS. Intracellular detection of cytoplasmic proteins was performed using the Intracellular Fixation & Permeabilization Buffer Set (Thermo Scientific). To stain nuclear proteins, we used the Foxp3/Transcription Factor Staining Buffer Set (Thermo Scientific). A FITC CaspaTag Pan-Caspase *In Situ* Assay Kit (EMD Millipore) was used to detect intracellular active caspases.

Mouse *i*NKT cells were defined as TCRβ$^+$PBS-57-loaded mCD1d tetramer$^+$ cells, and human *i*NKT cells as CD3$^+$PBS-57-loaded hCD1d tetramer$^+$ cells, while empty CD1d tetramers served as staining controls. Mouse MAIT cells were defined as B220$^-$TCRβ$^+$5-OP-RU-loaded mMR1 tetramer$^+$ cells, and human MAIT cells as CD3$^+$5-OP-RU-loaded hMR1$^+$ cells. 6-formylpterin (6-FP)-loaded MR1 tetramer reagents, which do not react with the *i*TCR of MAIT cells, were utilized in parallel as staining controls. We identified mouse T_{conv} cells as TCRβ$^+$PBS-57-loaded mCD1d tetramer$^-$ cells, and human T_{conv} cells as CD3$^+$PBS-57-loaded hCD1d tetramer$^-$5-OP-RU-loaded hMR1 tetramer$^-$ cells. Mouse NK cells, B cells and DCs were immunophenotyped as TCRβ$^-$NK1.1$^+$, TCRβ$^-$B220$^+$ and TCRβ$^-$CD11c$^+$ cells, respectively. Staining with isotype controls was used to draw gates as appropriate.

The fluorochrome-conjugated mAbs and tetramer reagents employed in this study are listed in the Key Resources Table. Cells were interrogated using a BD FACSCanto II flow cytometer equipped with BD FACSDiva version 6.1.2 software.

Quantitative PCR analyses

Hepatic *i*NKT and/or T_{conv} cells from ≥ 5 stressed or control mice were sorted to 100% purity using a BD FACSAria III Cell Sorter. Total RNA was isolated using a PureLink RNA Mini Kit (Thermo Scientific), and cDNA was synthesized using a SuperScript VILO cDNA Synthesis Kit (Thermo Scientific). Taqman Fast Advanced Master Mix (Applied Biosystems) was added to each cDNA sample, and the resulting mixture was plated in Custom Taqman Array Fast Plates (Thermo Scientific) containing probe/primer sets listed in Table S1. Cycle threshold (Ct) values from amplified transcripts were generated using a StepOne Plus Real-Time PCR instrument (Applied Biosystems). Normalized Ct (ΔCt) values were calculated by subtracting each Ct value by that of *Actb* and/or *Tbp*. The following formula was used to determine the relative mRNA content of the cells: Fold Change = $2^{-(\Delta\Delta Ct)}$.

Generation of bone marrow-derived dendritic cells (BMDCs)

Marrow cells were flushed out of femurs and tibias of B6 mice and depleted of erythrocytes. Cells were then washed, filtered and placed inside a T75 polystyrene flask at a density of 1 × 10^6 cells/mL of complete medium supplemented with 10 ng/mL each of recombinant mouse GM-CSF and IL-4 (Peprotech, Rocky Hill, NJ). Cultures were maintained for 6 days at 37°C in a humidified atmosphere containing 6% CO_2. Every other day, non-adherent cells were discarded, and cultures were replenished with fresh medium, GM-CSF and IL-4. Upon completion of the culture, cells were harvested using a cell scraper and CD11c$^+$ BMDCs were magnetically enriched using an EasySep Mouse CD11c Positive Selection Kit II (STEMCELL Technologies).

Ex vivo and *in vitro* treatments and stimulations

DN32.D3 cells were seeded at 1 × 10^5 cells/well of a U-bottom microplate and treated for 20 minutes with NE (0.1-10 μM) or NPY (10^{-6}-1 μM), both from Sigma-Aldrich, before they were stimulated with 100 ng/mL of αGC. Where indicated, cells were pretreated with 10 μM propranolol hydrochloride (Sigma-Aldrich) for 20 minutes before they were exposed to NE. After 24 h at 37°C, cell viability was assessed by 7-AAD staining, and the IL-2 content of supernatants was measured by ELISA.

Hepatic mouse *i*NKT cells were FACS-sorted from ≥ 5 stressed animals or controls. In a U-bottom microplate, *i*NKT cells were mixed with purified CD11c$^+$ BMDCs at an *i*NKT:DC ratio of 2:1. Co-cultures were stimulated with 100 ng/mL of αGC for 24 h at 37°C, after which cell-free supernatants were stored at −20°C for subsequent cytokine measurements.

In indicated experiments, HMNCs and splenocytes were seeded at 5 × 10^5 cells/well in a microplate and stimulated with 15 ng/mL of PMA plus 500 ng/mL of ionomycin in the presence of 10 μg/mL brefeldin A, all of which were purchased from Sigma-Aldrich. After 2 h at 37°C, cells were washed and stained for intracellular cytokines.

Hydrocortisone (HC) and dexamethasone (DEX) were purchased from Sigma-Aldrich, dissolved in absolute ethanol and diluted in RPMI 1640. In a U-bottom microplate, 1 × 10^5 human HMNCs/well or 5 × 10^5 human PBMCs/well were incubated for 24 h at 37°C in complete medium containing 0.01-10 μM HC or DEX.

51-chromium (^{51}Cr) release assay

YAC-1 target cells were incubated for 90 minutes at 37°C with 100 μCi $Na_2{}^{51}CrO_4$ (PerkinElmer). Labeled target cells were washed and then co-cultured at indicated effector:target ratios with splenocytes from stressed or control B6 mice that had received αGC or vehicle 24 hours before cytotoxicity assays. Cell-free supernatants were collected 4 h later, in which the ^{51}Cr activity was quantified using a PerkinElmer Wizard 1470 Automatic Gamma Counter. Experimental release (ER) values were obtained from wells in which effector and target cells were both present. Spontaneous release (SR) and total release (TR) were measured from wells containing medium alone or 1% Triton X-100, respectively. Cytotoxicity was calculated using the following formula: % specific lysis = [(ER-SR) ÷ (TR-SR)] × 100.

In vivo killing assay

Donor splenocytes from WT B6 and β2M$^{-/-}$ mice were labeled with 0.2 μM and 2 μM 5-(and-6)-carboxyfluorescein diacetate *N*-succinimidyl ester (CFSE), respectively, and used as target cells. Cells were washed, mixed at a 1:1 ratio, and analyzed by flow cytometry before injection. Approximately 1 × 10^7 cells from the resulting suspension were injected i.v. into stressed recipients that were treated with αGC or vehicle. Two h later, animals were sacrificed for their spleen in which the remaining CFSE^{hi} and CFSE^{lo} target cells were traced by flow cytometry. *In vivo* killing was calculated using the following formula: % specific killing = {1 - [(CFSE^{hi} events in recipient ÷ CFSE^{lo} events in recipient) ÷ (CFSE^{hi} events pre-injection ÷ CFSE^{lo} events pre-injection)]} × 100 as we previously described (Choi et al., 2019).

Metastatic melanoma model

Six h after administration of αGC or vehicle, stressed and control B6 mice received between 2.5 × 10^5 – 1 × 10^6 B16-F10 cells in 200 μL PBS i.v. Fourteen days later, lungs were harvested for digital imaging, and distinct tumor nodules on each lung were visually counted. Lungs harboring > 400 nodules were deemed to carry too many nodules for accurate enumeration. Therefore, they were conservatively represented as containing at least 400 nodules.

As an alternative method of measuring the metastatic tumor burden, B6 albino mice were injected with 5 × 10^5 B16-FLuc cells. After 21 days, they were anaesthetized with isoflurane and injected i.p. with 3 mg XenoLight D-Luciferin (PerkinElmer) in PBS. For up to 35 minutes thereafter, whole body bioluminescence imaging was conducted in an IVIS Lumina XRMS *In Vivo* Imaging System (PerkinElmer).

QUANTIFICATION AND STATISTICAL ANALYSIS

Flow cytometry results were analyzed using FlowJo version 10.0.7 software (Tree Star, Ashland, OR). The relative pixel intensities of bands in western blot images were quantified using Image Studio version 3.1.4 software. For bioluminescence imaging, total signal (photons/second/cm^2/steradian) was quantified by region-of-interest analysis using LivingImage software (PerkinElmer).

Throughout this investigation, objective quantification methods, as opposed to subjective scoring, were used. Therefore, blinding was not necessary. Sufficient sample sizes were not statistically predetermined but were consistent with those from comparable studies and based on our prior experience.

Student's t tests or one- or two-way ANOVA were employed, as appropriate, using GraphPad Prism version 6.0 software (La Jolla, CA). *, **, *** and **** denote statistically significant differences with $p < 0.05$, $p < 0.01$, $p < 0.001$ and $p < 0.0001$, respectively. Details related to sample sizes, measures of dispersion and the specific statistical tests used can be found in figure legends.

Cell Reports, Volume *35*

Supplemental information

Chronic stress physically spares but functionally impairs innate-like invariant T cells

Patrick T. Rudak, Joshua Choi, Katie M. Parkins, Kelly L. Summers, Dwayne N. Jackson, Paula J. Foster, Anton I. Skaro, Ken Leslie, Vivian C. McAlister, Vijay K. Kuchroo, Wataru Inoue, Olivier Lantz, and S.M. Mansour Haeryfar

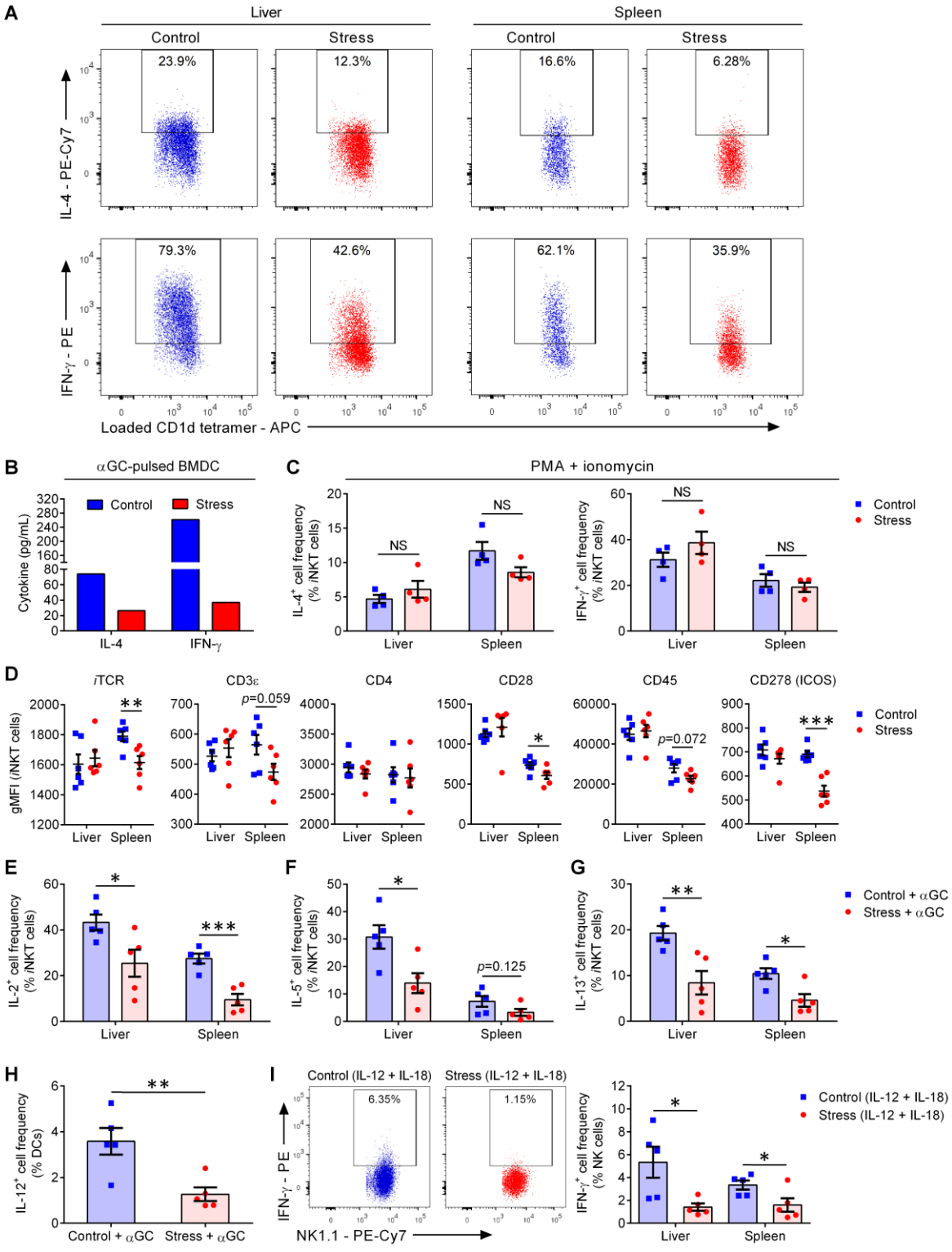

Supplemental Figure 1. Prolonged physical restraint impairs the ability of *i*NKT cells to elicit T_H1 and/or T_H2-type cytokine responses to αGC or to a combination of IL-12 and IL-18, but not to a combination of PMA

and ionomycin (related to Figure 1). (A) B6 mice were physically restrained (or not) for 12 h before they were given αGC. Two hours later, HMNCs and splenocytes were stained with mAbs against IL-4 and IFN-γ and analyzed by flow cytometry. Representative dot plots illustrate the frequencies of IL-4$^+$ and IFN-γ$^+$ *i*NKT cells after gates were set based on isotype control staining. **(B)** Sorted hepatic *i*NKT cells pooled from ≥5 stressed or control B6 mice were stimulated *ex vivo* with 100 ng/mL of αGC in the presence of CD11c$^+$ BMDCs. After 24 h, IL-4 and IFN-γ levels in culture supernatants were measured. **(C)** HMNCs and splenocytes from stressed and control B6 mice were stimulated for 2 h with 15 ng/mL of PMA and 500 ng/mL of ionomycin before intracellular levels of IL-4 and IFN-γ in *i*NKT cells were determined by flow cytometry. **(D)** HMNCs and splenocytes from restrained or control animals were stained with loaded CD1d tetramer or mAbs against indicated molecules. After gating on *i*NKT cells, the gMFI of staining for each molecule is depicted. **(E-G)** As in (**A**), but summary data indicates the frequencies of *i*NKT cells staining positively for mAbs against IL-2 **(E)**, IL-5 **(F)** and IL-13 **(G)**. **(H)** B6 mice were restrained (or not) for 12 h before they were given αGC. Six h later, HMNCs were stained with an anti-IL-12p35 mAb or a rat IgG2aκ isotype control. The frequency of IL-12$^+$ DCs was determined after gating on TCRβ$^-$CD11c$^+$ events. **(I)** Mice that had been restrained or left undisturbed were injected with IL-12 and IL-18 one h before the percentages of IFN-γ$^+$ events among TCRβ$^-$NK1.1$^+$ NK cells were determined. Representative flow plots and summary data are shown. Each symbol represents an individual mouse, and error bars represent SEM. *, ** and *** denote significant differences with $p<0.05$, $p<0.01$ and $p<0.001$, respectively, by unpaired Student's *t*-tests. NS = not significant

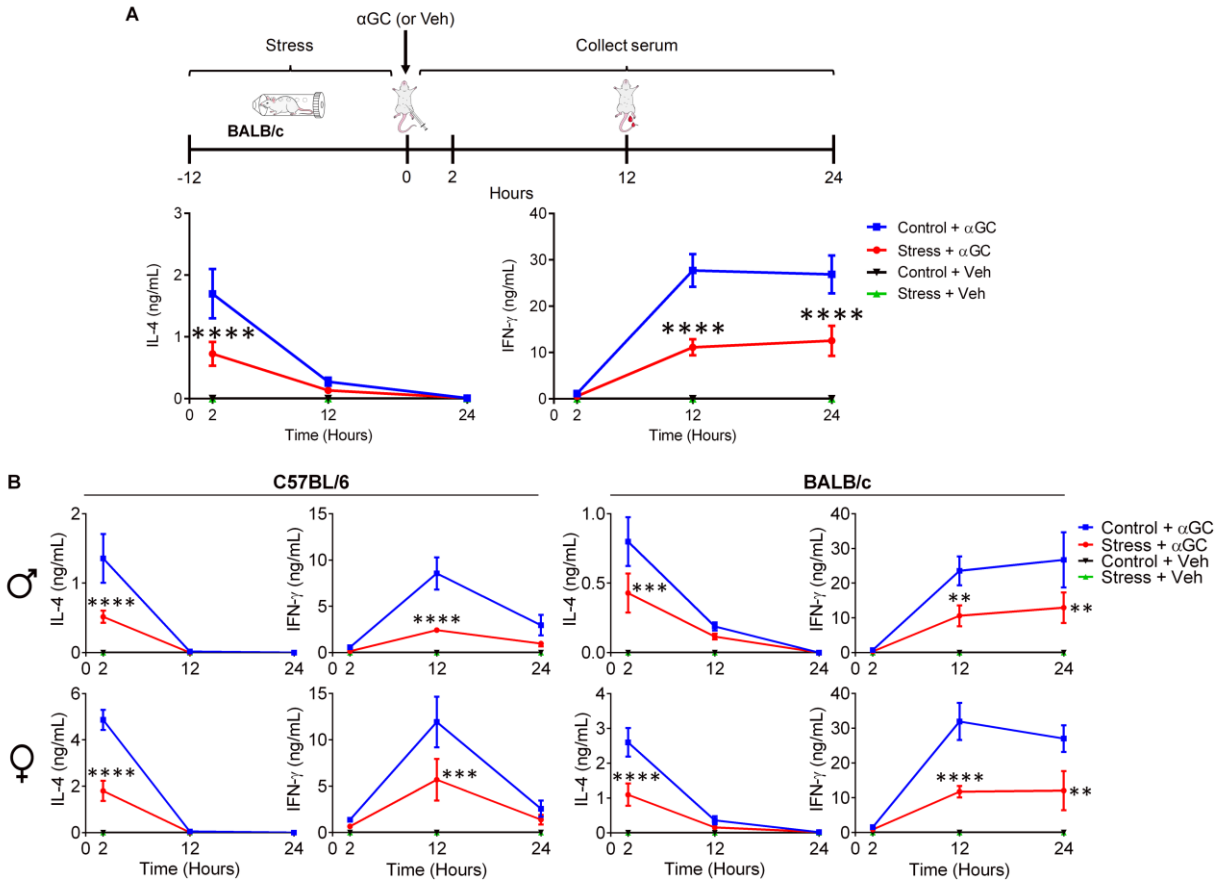

Supplemental Figure 2. Prolonged stress impairs cognate *i*NKT cell responses in male and female B6 and BALB/c mice (related to Figure 1). (A) WT BALB/c mice were subjected to physical restraint or left undisturbed for 12 h before they were injected i.p. with αGC or Veh. At indicated time points, IL-4 and IFN-γ in serum samples were quantified by ELISA (n=8-9/group). **(B)** Data presented in Figure 1B-C and Figure S2A were segregated by sex. The kinetics of serum cytokine levels following αGC (or Veh) administration in male (B6: n=5; BALB/c: n=5) and female (B6: n=5; BALB/c: n=3-4) mice are depicted. Error bars represent SEM. **, *** and **** denote differences with $p<0.01$, $p<0.001$ and $p<0.0001$, respectively, using two-way ANOVA with Dunnett's post-hoc analysis.

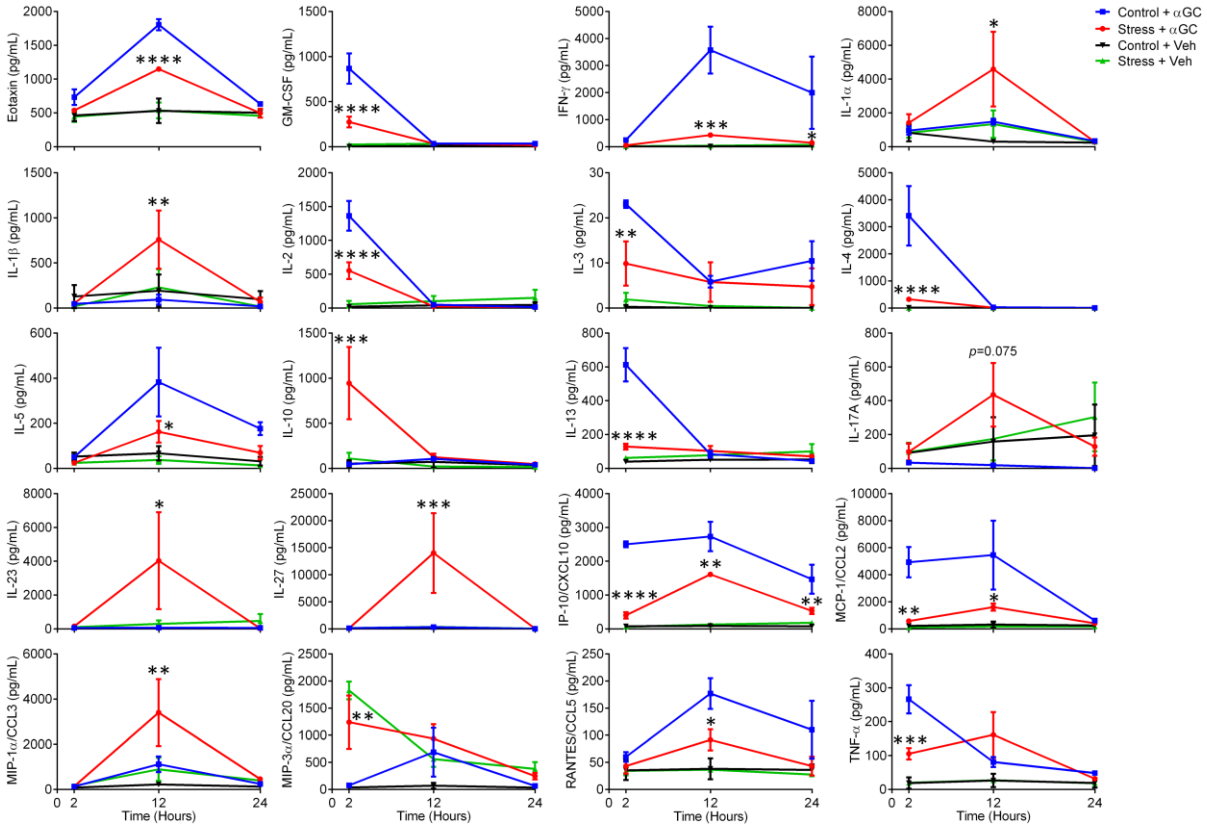

Supplemental Figure 3. Prolonged physical restraint before αGC administration alters the serum concentrations of a wide range of inflammatory mediators (related to Figure 1). WT B6 mice were restrained or left undisturbed for 12 h before they were injected with αGC or Veh (n=3/cohort). Two, 12 and 24 h later, mice were bled and serum levels of indicated mediators were quantified by cytokine/chemokine multiplexing. *, **, *** and **** denote significant differences between stressed and control animals receiving αGC with $p<0.05$, $p<0.01$, $p<0.001$ and $p<0.0001$, respectively, using two-way ANOVA with Tukey's post-hoc analysis.

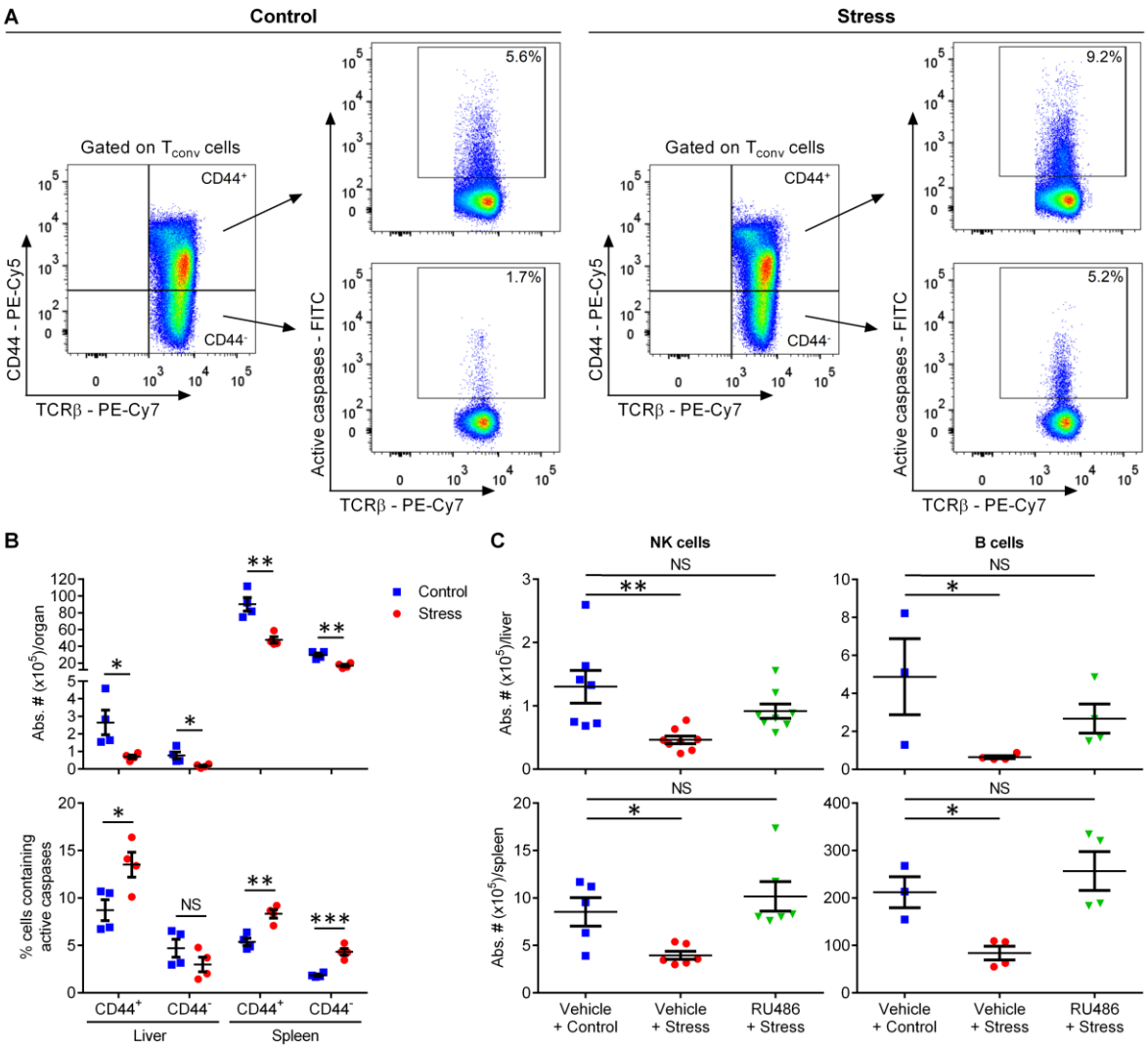

Supplemental Figure 4. Unlike *i*NKT cells, naïve and memory T_{conv} cells, NK cells and B cells are prone to stress-induced apoptosis (related to Figure 2). (A-B) Splenocytes and HMNCs from restrained and control B6 mice were stained for surface TCRβ, surface CD44 and intracellular active caspases. A rat IgG2bκ isotype control was used to set the gate for CD44 staining. **(A)** Representative FACS plots illustrate our gating strategy to distinguish between splenic $CD44^+$ and $CD44^-$ populations among $TCR\beta^+CD1d$ tetramer$^-$ events, which correspond to memory and naïve T_{conv} cells, respectively. Gates containing T_{conv} cells with intracellular active caspases are also shown. **(B)** The absolute numbers of hepatic and splenic memory and naïve T_{conv} cells and the percentages of T_{conv} cells staining positively for active caspases are depicted. **(C)** Separate cohorts of B6 mice were treated i.p. with RU486 or Veh.

One hour later, animals were subjected to prolonged restraint stress or were left undisturbed for 12 h. HMNCs and splenocytes were prepared shortly afterwards and stained with a panel of mAbs against TCRβ, NK1.1 and B220. $TCR\beta^{-}NK1.1^{+}$ NK cells and $TCR\beta^{-}B220^{+}$ B cells were identified by flow cytometry, and their absolute numbers were calculated. Each symbol represents an individual mouse, and error bars represent SEM. *, ** and *** denote differences with $p<0.05$, $p<0.01$ and $p<0.001$, respectively, using unpaired Student's *t*-tests (**B**) or one-way ANOVA with Dunnett's post-hoc analysis (**C**). NS = not significant

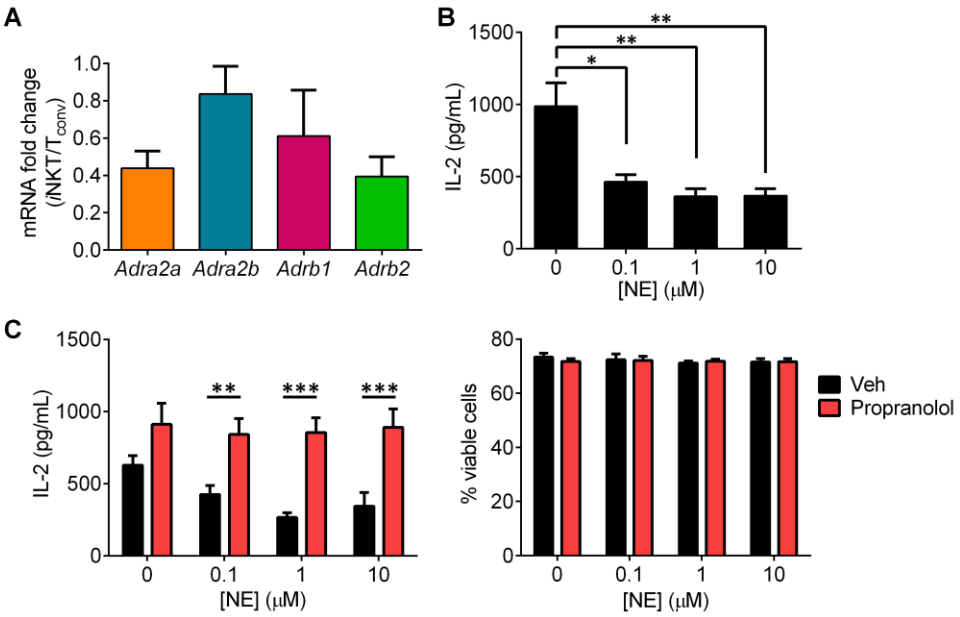

Supplemental Figure 5. *i*NKT cells express adrenergic receptors and respond weakly to αGC in the presence of NE in an *in vitro* setting (related to Figure 3). (A) HMNCs from 10 naïve B6 mice were pooled and co-stained with an anti-TCRβ mAb and PBS-57-loaded CD1d tetramers. *i*NKT and T_{conv} cells were FACS-purified for cDNA synthesis and gene expression analysis by quantitative PCR. The expression of indicated genes by *i*NKT cells relative to T_{conv} cells was calculated using the $2^{-(\Delta\Delta Ct)}$ method. Data from 3 independent experiments were used to determine fold change values. **(B)** DN32.D3 cells were exposed for 20 minutes to indicated concentrations of norepinephrine (NE) before they were stimulated with 100 ng/mL of αGC. The IL-2 content of culture supernatants was quantified after 24 h by ELISA (n=3-5). **(C)** DN32.D3 cells were pretreated for 20 minutes with propranolol before they were exposed to NE and subsequently stimulated with αGC (n=4). After 24 h, IL-2 was measured in supernatants (n=4) and cellular viability was assessed by 7-AAD staining (n=3). Error bars represent SEM. *, ** and *** denote differences with $p<0.05$, $p<0.01$ and $p<0.001$, respectively, by one-way ANOVA with Dunnett's post-hoc analysis (**B**) or by unpaired Student's *t*-tests (**C**).

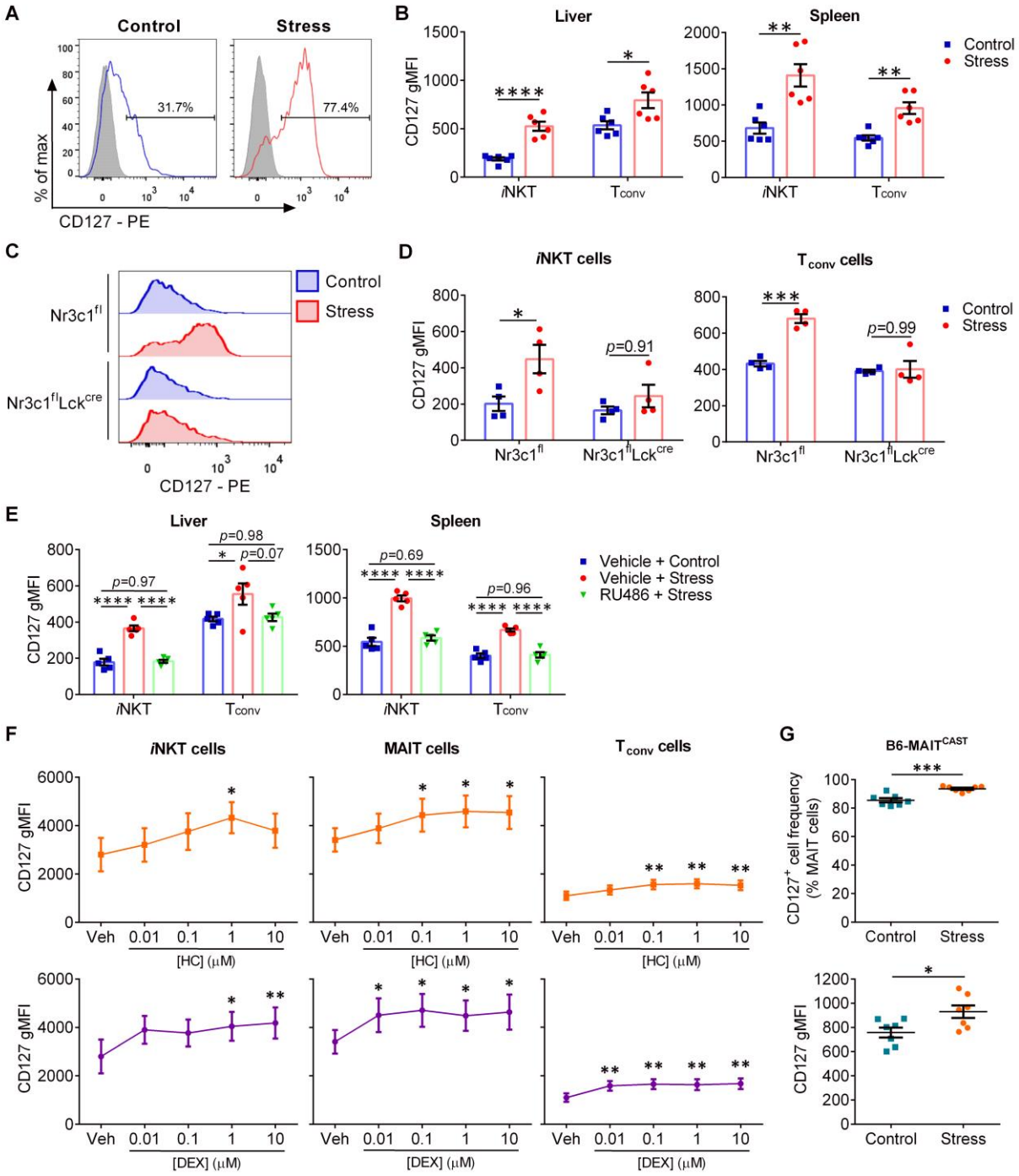

Supplemental Figure 6. Mouse and human *i*NKT, MAIT and T_{conv} cells upregulate CD127 in response to GR signaling (related to Figure 7). B6 mice were subjected to 12 h of restraint stress (or not). Shortly afterwards, HMNCs and splenocytes were prepared and stained to detect CD127 expression on the surface of *i*NKT and T_{conv}

cells. Open and filled histograms correspond to staining with an anti-CD127 mAb and a rat IgG2aκ isotype control, respectively, after gating on hepatic *i*NKT cells **(A)**. Cumulative data depicting the gMFI of CD127 staining in indicated populations are also shown **(B)**. $Nr3c1^{fl}$ and $Nr3c1^{fl}Lck^{cre}$ mice were physically restrained (or not) and assessed for CD127 expression in their *i*NKT and T_{conv} cell compartments **(C-D)**. Blue and red histograms correspond to CD127 expression on hepatic *i*NKT cells from control and stressed mice, respectively **(C)**, and cumulative data for indicated cell populations are summarized using bar graphs **(D)**. Separate cohorts of WT B6 mice received RU486 (or Veh) i.p. 1 h before they were physically restrained (or not). The gMFI of CD127 staining is shown **(E)**. Human PBMCs were cultured for 24 h in the presence of hydrocortisone (HC), dexamethasone (DEX) or vehicle before they were stained with either an anti-CD127 mAb or a mouse IgG1κ isotype control. The gMFI of CD127 staining in *i*NKT, MAIT and T_{conv} cells was assessed by flow cytometry (n=5) **(F)**. B6-$MAIT^{CAST}$ mice were physically restrained or left undisturbed for 12 h before they were sacrificed for their liver. HMNCs were stained with a mAb to CD127 or a rat IgG2aκ isotype control. After gating on $TCR\beta^{+}B220^{-}$MR1 $tetramer^{+}$ MAIT cells, the percentages of $CD127^{+}$ cells and the gMFI of CD127 staining were determined **(G)**. Each symbol in (**B**, **D**-**E** and **G**) represents an individual mouse. Error bars represent SEM. *, **, *** and **** denote differences with $p<0.05$, $p<0.01$, $p<0.001$ and $p<0.0001$, respectively, using unpaired Student's *t*-tests (**B**, **D** and **G**) or one-way ANOVA (**E**-**F**).

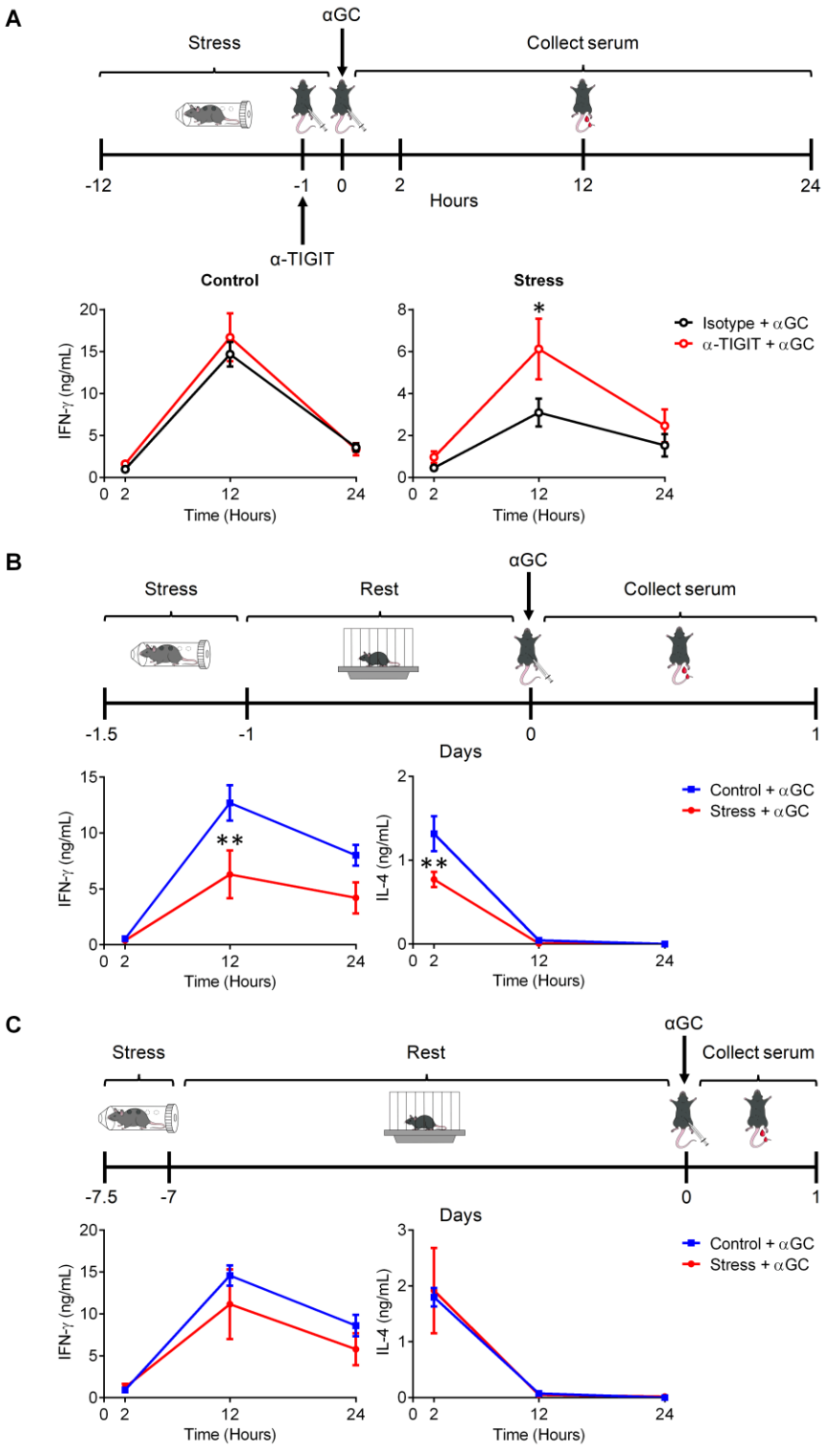

Supplemental Figure 7. Stress-induced *i*NKT cell impairments are partially mediated by TIGIT and do not last long after the stressor is removed (related to Figure 4). (A) B6 mice were restrained or left undisturbed

before they received a 200-μg i.p. dose of an anti-mouse TIGIT mAb (or a mouse IgG1κ isotype control) followed by αGC administration as schematically illustrated. Mice were bled at indicated time points, and serum IFN-γ levels were quantified (n=8-9/group). **(B-C)** Separate cohorts of B6 mice were physically restrained or left undisturbed for 12 h. Mice were then returned to standard housing conditions for one day **(B)** or seven days **(C)** before they were injected i.p. with αGC. Serum IFN-γ and IL-4 levels were measured at indicated time points (n=4/group). Error bars represent SEM. * and ** denotes differences with $p<0.05$ and $p<0.01$, respectively, using two-way ANOVA with Sidak's post-hoc analysis.

Supplemental Table 1: Taqman-based qPCR primer/probe sets used in this study (related to STAR Methods).

Target	Assay Identification
Abl1	Mm00802029_m1
Actb	Mm00607939_s1
Adra1a	Mm00442668_m1
Adra1b	Mm00431685_m1
Adra1d	Mm01328600_m1
Adra2a	Mm00845383_s1
Adra2b	Mm00477390_s1
Adra2c	Mm00431686_s1
Adrb1	Mm00431701_s1
Adrb2	Mm02524224_s1
Adrb3	Mm02601819_g1
Aifm1	Mm00442540_m1
Anxa5	Mm01293059_m1
Apaf1	Mm01223702_m1
Api5	Mm00500189_m1
Atf5	Mm04179654_m1
Bad	Mm00432042_m1
Bag1	Mm01208593_m1
Bag3	Mm00443474_m1
Bak1	Mm00432045_m1
Bax	Mm00432051_m1
Bbc3	Mm00519268_m1
Bcl2	Mm00477631_m1
Bcl2a1a	Mm03646861_mH
Bcl2l1	Mm00437783_m1
Bcl2l11	Mm00437796_m1
Bid	Mm00432073_m1
Bik	Mm00476123_m1
Birc2	Mm00431811_m1
Birc3	Mm01168413_m1
Birc5	Mm00599749_m1
Bmf	Mm00506773_m1
Bnip2	Mm00443990_m1
Card10	Mm00459941_m1
Card6	Mm01297056_m1
Casp1	Mm00438023_m1
Casp2	Mm00432314_m1
Casp3	Mm01195085_m1
Casp4	Mm00432307_m1
Casp6	Mm00438053_m1
Casp7	Mm00432324_m1
Casp8	Mm00802247_m1
Casp9	Mm00516563_m1
Cblb	Mm01343092_m1

Cd27	Mm01185212_g1
Cd28	Mm00483137_m1
Cd40lg	Mm00441911_m1
Cd44	Mm01277161_m1
Cd69	Mm01183378_m1
Cd274	Mm03048248_m1
Cdk2	Mm00443947_m1
Cdk4	Mm00726334_s1
Cflar	Mm01255578_m1
Cradd	Mm01226172_m1
Csf1	Mm00432686_m1
Dad1	Mm01319221_m1
Dffa	Mm00438410_m1
Dffb	Mm00432822_m1
Diablo	Mm01194441_m1
Egr2	Mm00456650_m1
Egr3	Mm00516979_m1
Fadd	Mm00438861_m1
Fas	Mm01204974_m1 Mm00433237_m1
Fasl	Mm00438864_m1
Fos	Mm00487425_m1
Foxo3	Mm01185722_m1
Foxp1	Mm00474848_m1
Gata3	Mm00484683_m1
Gzma	Mm01304452_m1
Gzmb	Mm00442834_m1
Hells	Mm00468580_m1
Icam1	Mm00516023_m1
Icos	Mm00497600_m1
Ifng	Mm01168134_m1
Ifnar1	Mm00439544_m1
Ifnar2	Mm00494916_m1
Igf1r	Mm00802831_m1
Il10ra	Mm00434151_m1
Il12rb1	Mm00434189_m1
Il18rap	Mm00516053_m1
Il2	Mm00434256_m1
Il2ra	Mm01340213_m1
Il2rb	Mm00434268_m1
Il4	Mm00445259_m1
Il7ra/Cd127	Mm00434295_m1
Irf4	Mm00516431_m1
Itch	Mm01246513_m1
Jak1	Mm00600614_m1
Jak3	Mm00439962_m1
Jun	Mm00495062_s1

Lat	Mm00456761_m1
Lta	Mm00440228_gH
Myb	Mm00501741_m1
Naip2	Mm00440446_m1
Nfatc1	Mm00479445_m1
Nfatc2	Mm00477776_m1
Nfatc3	Mm01249200_m1
Nfkb1	Mm00476361_m1
Notch1	Mm00435249_m1
Npy1r	Mm04208490_m1
Npy2r	Mm01218209_m1
Npy4r	Mm01220859_m1
Npy5r	Mm00443855_m1
Npy6r	Mm00627550_m1
Nr3c1	Mm00433832_m1
Nr4a1	Mm01300401_m1
Pim2	Mm00454579_m1
Pmaip1	Mm00451763_m1
Polb	Mm00448234_m1
Prf1	Mm00812512_m1
Ptger2	Mm00436051_m1
Ripk1	Mm00436354_m1
Rnf128	Mm00480990_m1
Sell	Mm00441291_m1
Sphk2	Mm00445021_m1
Stat3	Mm01219775_m1
Stat6	Mm01160477_m1
Tbp	Mm00446973_m1
Tbx21	Mm00450960_m1
Tgfb1	Mm01178820_m1
Tnfa	Mm00443258_m1
Tnfrsf10b	Mm00457866_m1
Tnfrsf14	Mm00619239_m1
Tnfrsf4	Mm00442039_m1
Tnfrsf9	Mm00441899_m1
Tnfsf10	Mm01283606_m1
Tnfsf14	Mm00444567_m1
Tnfsf8	Mm00437153_m1
Traf1	Mm00493827_m1
Traf2	Mm00801978_m1
Traf3	Mm00495752_m1
Trp53bp2	Mm00557629_m1
Xiap	Mm01311594_mH
Zbtb16	Mm01176868_m1
Zc3hc1	Mm01168068_m1